NASA TECHNICAL MEMORANDUM

UB
NASA TM X-1213

PERFORMANCE CHARACTERISTICS OF AN AXIAL-FLOW LIQUID-HYDROGEN PUMP DURING STARTUP

by Wojciech Rostafinski, Richard A. Rudey, Donald D. Lacy, and Patrick R. Lillis

Lewis Research Center
Cleveland, Ohio

NATIONAL AERONAUTICS AND SPACE ADMINISTRATION • WASHINGTON, D. C. • FEBRUARY 1966

[redacted]

NASA TM X-1213

PERFORMANCE CHARACTERISTICS OF AN AXIAL-FLOW LIQUID-HYDROGEN PUMP DURING STARTUP

By Wojciech Rostafinski, Richard A. Rudey, Donald D. Lacy, and Patrick R. Lillis

Lewis Research Center
Cleveland, Ohio

NATIONAL AERONAUTICS AND SPACE ADMINISTRATION

[redacted]

PERFORMANCE CHARACTERISTICS OF AN AXIAL-FLOW LIQUID-HYDROGEN PUMP DURING STARTUP

by Wojciech Rostafinski, Richard A. Rudey,
Donald D. Lacy, and Patrick R. Lillis

Lewis Research Center

SUMMARY

The pressure drop and torque characteristics of an axial-flow liquid-hydrogen pump during pressurized start were studied both analytically and experimentally. The experimental characteristics were obtained for zero speed, breakaway, and windmilling operation, using a Rocketdyne Mark IX turbopump assembly installed in a simulated full-scale nuclear rocket cold-flow system. The pump static pressure drop, rotational speed, and the zero speed and accelerating torque data were obtained as functions of liquid-hydrogen flow rate forced through the system under the action of tank pressure. These data are presented herein and the effects of the system on the results obtained are discussed. Analytical models for calculating the pressure drop and torque characteristics of pumps for extreme off-design operation are developed and presented as generalized equations.

Pressure drop and torque parameters are calculated, using the derived analytical models, for the subject pump over a wide range of operating conditions including the limiting cases of no rotation and steady windmilling (zero acceleration). Comparison between the experimental and calculated results indicate that it is possible to describe theoretically the pressure drop and torque characteristics of an axial-flow pump in this mode of operation.

Generalized pump (pressure rise and torque) characteristic curves constructed from known pump data in the high-speed region of operation are extrapolated to near zero speed. Comparison between the experimental and extrapolated results indicate that an approximate pressure-drop characteristic for zero speed and windmilling operation can be predicted using this technique without the need for a special test setup. An approximate zero-speed torque point can also be predicted from a torque extrapolation.

INTRODUCTION

In the development of nuclear rocket engine systems, the analog computer is being used to study the effects of engine-component performance characteristics on the overall system performance of the engine. Of particular importance

[redacted]

in these studies is the engine performance during the initial startup. Several parametric studies have been conducted by engine manufacturers (e.g., Aerojet-General Corporation, Pratt & Whitney Aircraft, and Rocketdyne Div. of NAA) to investigate the startup and control characteristics of nuclear engine systems. In addition, analog studies are currently being conducted at the NASA-Lewis Research Center. The results of these studies indicate that the component performance during the initial startup phase of operation must be accurately simulated in order to obtain meaningful results. Up to the present time, the turbopump performance in the startup cycle has been simulated by using an extrapolation of the normal operating characteristics because analytical models describing the startup characteristics were not available. In order to define component characteristics during initial engine startup, a full-scale cold-flow nuclear rocket experiment is currently being conducted by the Lewis Research Center. In addition to obtaining information regarding dynamic and heat-transfer phenomena throughout the system and its components, one of the primary objectives of this experiment is to define the startup performance of turbopumps and to develop analytical models representing their characteristics.

One segment of the experimental investigation that is being conducted has produced data concerning pump operating characteristics as a result of initiating flow through the simulated engine system under various run tank pressure conditions without supplying power to the turbine. The turbopump assembly used was the Rocketdyne Mark IX unit which is described in the APPARATUS AND INSTRUMENTATION section of this report.

In conjunction with the experimental investigation, an analytical investigation was conducted to determine the zero speed and windmilling performance of a pump as functions of flow rate being forced through the pump under the action of tank pressure. Since at windmilling, the pump acts as a turbine, equations are developed for a multistage axial-flow hydraulic turbine for operation at extreme off-design conditions. Because of uncertainties in evaluating the flow deviation angles and internal blockage, due to the negative incidence and the boundary layer considerations, a parametric study of these factors was conducted. Equations pertaining to the pump pressure drop, the available fluid torque, and the turbopump accelerating torque are developed as functions of a speed parameter.

The purpose of this report is to present and compare the results of the analytical and experimental investigations in order to determine the accuracy and usefulness of the analytical models. In addition, descriptions of the test facility, the full-scale nuclear rocket engine cold-flow system, the system operating procedures, and the data acquisition and reduction system are presented in order to furnish a reference for future reports emanating from the cold-flow experiment.

The studies were conducted utilizing the B-1 test facility located at the NASA Plum Brook Station.

[redacted]

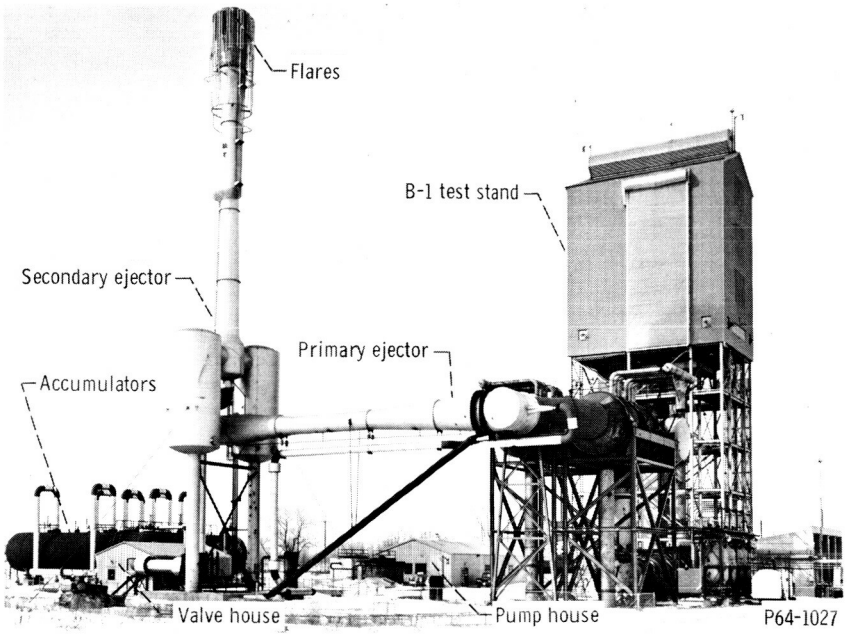

Figure 1. - B-1 test facility.

APPARATUS AND INSTRUMENTATION

Facility

The test facility (see fig. 1) consists of a vertical tower with a height of 135 feet and a base of 34 by 42 feet. The test stand is enclosed above the 68-foot level with roll-up doors on the north, south, and west sides. The doors are required to provide adequate ventilation in the event of a hydrogen leak. Two open floor areas below the 68-foot level are used for some of the auxiliary systems. A concrete shelter for liquid-hydrogen Dewar parking is located at the base of the test stand. Adjacent to this is the instrumentation terminal room, relay cabinets, and a limited working area for the facility personnel.

The facility includes an altitude exhaust system which is capable of providing a minimum pressure (zero flow) of 0.5 pound per square inch for 4 minutes at the research system exhaust nozzle exit. The gaseous-hydrogen pumping capacity of this system is 10, 20, 30, and 48 pounds per second with exhaust nozzle exit pressures of 1.5, 4, 8, and 14.7 pounds per square inch, respectively. A no-flow ejector below the nozzle exit is used to maintain low nozzle-exhaust back pressure.

At present, two liquid Dewars, four gas trailers, and 100 000 standard cubic feet of permanent gas storage constitute the gaseous and cryogenic farm system. The mobile Dewars, one liquid nitrogen and the other liquid hydrogen, are self-pressurizing, multiple-outlet types with a 6000-gallon maximum capacity. There are two gaseous hydrogen trailers, one gaseous helium trailer and one gaseous nitrogen trailer each having a capacity of 70 000 standard cubic feet at 2400 pounds per square inch pressure. The permanent storage bottles contain gaseous nitrogen with an operating pressure of 2400 pounds per square inch for purging the altitude exhaust duct.

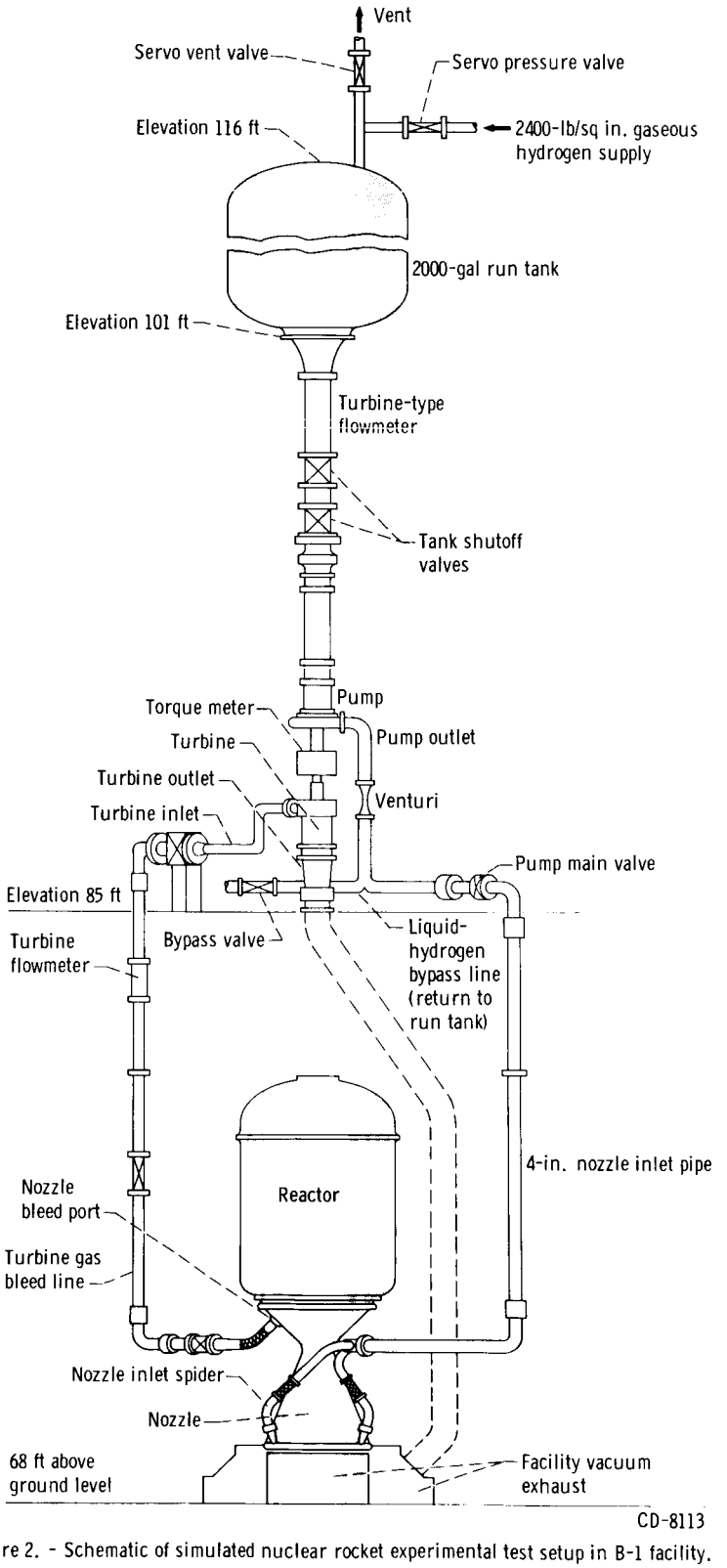

Figure 2. - Schematic of simulated nuclear rocket experimental test setup in B-1 facility.

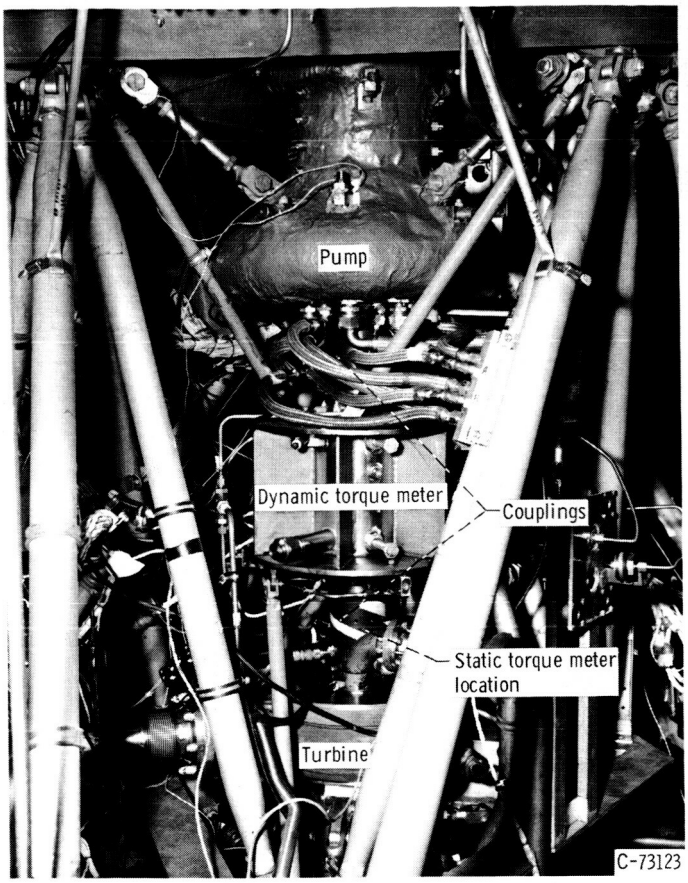

Figure 3. - Mark-IX liquid-hydrogen turbopump installed in mount.

Research System

The research apparatus is located within the enclosed area of the test stand and consists of a tank, turbopump, reactor, and exhaust nozzle in a system configuration as shown schematically in figure 2.

The run tank has a maximum capacity of 2000 gallons of liquid hydrogen. It has a length of 15 feet, and a diameter of 5 feet. The tank is insulated with 4 inches of polyurethane insulation and is designed for operating pressures up to 100 pounds per square inch.

At the bottom outlet of the tank is a liquid-hydrogen anti-swirl vane assembly followed by a wire-mesh filter below a converging transition spool. Downstream of the filter, the liquid hydrogen flows through straightening vanes before entering a 4-inch flowmeter. The ducting below the flowmeter is 8 inches in diameter. The inlet ducting from the tank discharge to the pump inlet $\left(8\frac{1}{2}\text{ ft long}\right)$ also contains two 8-inch butterfly valves in series. The upstream valve is a pneumatically operated open and close facility tank shutoff valve and the downstream valve is a servohydraulically operated control valve.

The turbopump assembly installed in its mount is shown in figure 3. The pads of the tripod mounting frame are bolted to large facility I beams for stable mounting.

The pump discharge to nozzle inlet manifold section of the system is a 4-inch-nominal-diameter duct. This line contains a Venturi flowmeter, a bypass line connected to the tank, a 4-inch servooperated butterfly control valve, a bleed line ventable to atmosphere, and a dump line connected to the ejector system to allow disposal of chilldown fluid when required. The line is extensively instrumented and insulated with a foam-in-place insulation.

Approximately 18 feet downstream from the main pump discharge flow-control valve, the propellant line is divided equally into three $2\frac{3}{8}$-inch-diameter ducts (spider) which feed the nozzle inlet manifold of an RN-2 regeneratively cooled, tubular-wall nozzle. The nozzle is attached to a modified KIWI-B-1B cold-flow reactor which utilizes unloaded fuel elements, fixed control rods, and dummy

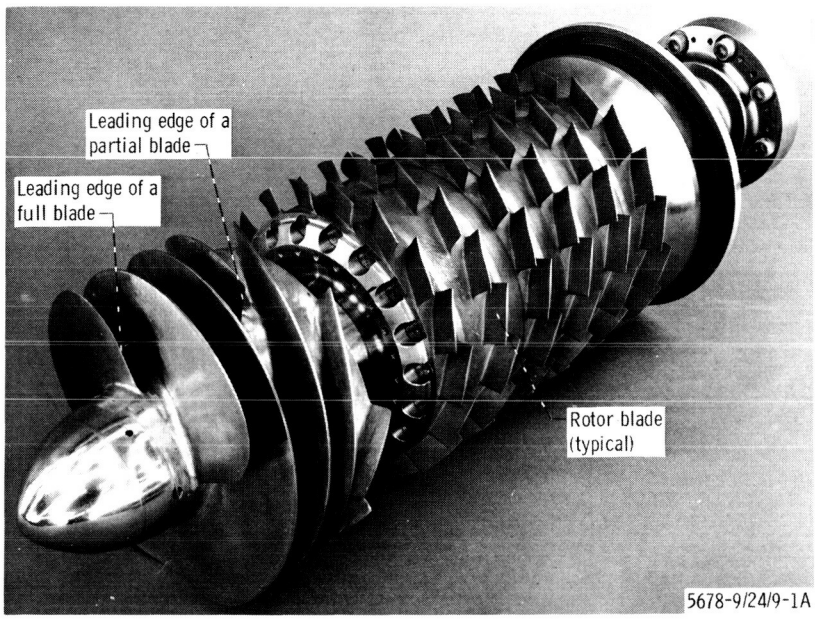

Figure 4. - Mark-IX pump rotor assembly.

TABLE I. - INDUCER STAGE GEOMETRY AND BLADE DESIGN VALUES

Parameter	Rotor	Stator
Inlet mean blade diameter, in.	5.125	6.60
Exit mean blade diameter, in.	6.60	6.60
Inlet annulus area, sq in.	34.21	12.96
Exit annulus area, sq in.	12.96	12.96
Chord at mean blade diameter, in.	8.0	1.89
Spacing at mean blade diameter, at exit, in.	2.59	1.10
Blade height, at exit, in.	.62	.62
Inlet hub-tip ratio	.414	.829
Exit hub-tip ratio	.829	.829
Blade clearance, in.	.010	-----
Blade solidity at tip	-----	1.51
Blade solidity at hub	-----	2.00
Number of blades	4-partial 4-full	19
Diffusion factor at tip	-----	.561
Diffusion factor at hub	-----	.519
Ideal head-rise coefficient at tip	.373	-----
Ideal head-rise coefficient at hub	.352	-----
Inlet flow coefficient	.098	-----
Exit flow coefficient	.253	-----
Incidence angle at tip, deg	2.2	-1.5
Incidence angle at hub, deg	5.4	-2.5
Deviation angle at tip, deg	.9	10
Deviation angle at hub, deg	1.3	10

control-rod actuators. The propellant enters the nozzle manifold, flows through 180 single-pass cooling-nozzle tubes and into the reflector inlet plenum of the reactor. It then flows upward through the reflector segments into the reactor dome then downward through the core and nozzle into the altitude exhaust system.

The nozzle has a hot-bleed port capable of supplying hydrogen gas to power the turbine for bootstrap operation. For the subject investigation, the ducts connecting the hot-bleed port to the turbine and the turbine to the altitude exhaust system were not connected.

The overall experimental assembly constitutes a reasonable simulation of a full-scale flight-type nuclear rocket engine configuration.

Turbopump Assembly

The Mark IX turbopump assembly consists of three separate components: (1) an axial-flow pump, (2) a dynamic torquemeter, and (3) an axial-flow turbine. The three components are mounted vertically in line using a tripod mounting frame which has the capability of individually positioning each component in order to obtain an accurate alinement. The three components are coupled together with two spline-gear couplings to form a direct-drive assembly. A photograph of this assembly installed in the mount is shown in figure 3. Complete descriptions of the individual components, including design requirements and analyses, are given in references 1 (axial-flow pump), 2 (turbine), and 3 (torquemeter). Descriptions regarding some of the salient design features which affect the overall performance of these components are given below.

Axial-flow pump. - The pump is composed of an axial-entrance, mixed-flow, axial-discharge inducer stage, six identical high-pressure axial-flow stages, and a single-outlet collecting volute. The pump is designed for pumping liquid hydrogen, is self-lubricated (using liquid hydrogen as the lubricating and cooling fluid for the bearings), and has a rotating balance piston to compensate for internal axial-thrust loads. A photograph of the pump inducer and axial rotor assembly is shown in figure 4.

The geometry and blade design values of the inducer stage are given in table I. The blade design values given are not the same as those given in reference 1 due to a reevaluation of blockage and blade interaction effects by the pump manufacturer. This reevaluation resulted in a 5 percent increase in axial velocity thus affecting the design-velocity vector diagrams. The inducer rotor blades are a varying pitch, helical configuration. The four partial blades begin at half the axial length along the hub. The inducer stator blades are a mean-line circular-arc design and machined integral with the housing used for the forward bearing support.

The geometry and blade design values of the six identical axial rotors and the five identical stators are given in table II. These blade design values also are based on the 5-percent increase in axial velocity as previously mentioned. The axial rotor blades are a mean-line circular-arc, free-vortex design and are machined integral with individual rotor disks. The actual head-rise coefficient of the unit used in the subject investigation is approximately

TABLE II. - AXIAL STAGE GEOMETRY AND BLADE DESIGN VALUES

Parameter	Rotor	Stator
Mean blade diameter (inlet and exit), in.	6.60	6.60
Annulus area (inlet and exit), sq in.	12.96	12.96
Chord at mean blade diameter, in.	1.39	.93
Spacing at mean blade diameter, in.	1.224	.495
Blade height, in.	.62	.62
Hub-tip ratio (inlet and exit)	.829	.829
Blade clearance, percent of blade height	4 at tip	4 at hub
Blade solidity at tip	1.035	1.86
Blade solidity at hub	1.25	1.90
Number of blades	17	42
Diffusion factor at tip	.384	.473
Diffusion factor at hub	.520	.536
Ideal head-rise coefficient (constant-hub to tip)	.260	-----
Flow coefficient (constant-hub to tip)	.295	-----
Incidence angle at tip, deg	-1	-3
Incidence angle at hub, deg	0	-2.5
Deviation angle at tip, deg	5	8
Deviation angle at hub, deg	6	8

10-percent lower than design due to increasing the blade-tip clearance from 2 percent of the blade height (ref. 1) to 4 percent (table II). The stator blades are a mean-line circular-arc design and are machined integral with a three-segment outer shroud. The rotor tips and the stator hubs are both unshrouded.

The single outlet volute has turning vanes and supporting members. The scroll cross sections, around the circumference, are designed to maintain a constant average velocity.

Dynamic torquemeter. - The dynamic torquemeter assembly is composed of a calibrated torque shaft with a 60-tooth rotor and spline at each end, two magnetic speed pickups and a finned housing containing two oil-lubricated bearings and two dynamic seals. During powered operation, shaft torque is determined from the angle of twist in the shaft which is obtained by measuring the phase angle difference between two signals generated by the toothed rotors and the magnetic pickups.

Turbine. - The turbine is a six-stage, pressure-compounded, axial-flow unit designed for operation using the products of combustion from an oxygen-hydrogen gas generator. A cutaway drawing of the turbine is shown in figure 5. The turbine stage geometry and design performance values are given in table III. Performance values are given for both design (oxygen-hydrogen) and hot hydrogen operation. The first, second, and third stage rotors have impulse blading and the fourth, fifth, and sixth stages have free-vortex blading. The blades are machined integral with the rotor disks. The working fluid enters the turbine through a single-entrance scroll and is discharged through an axial-core diffuser. Oil is used as a lubricant for the two roller and one ball bearing system.

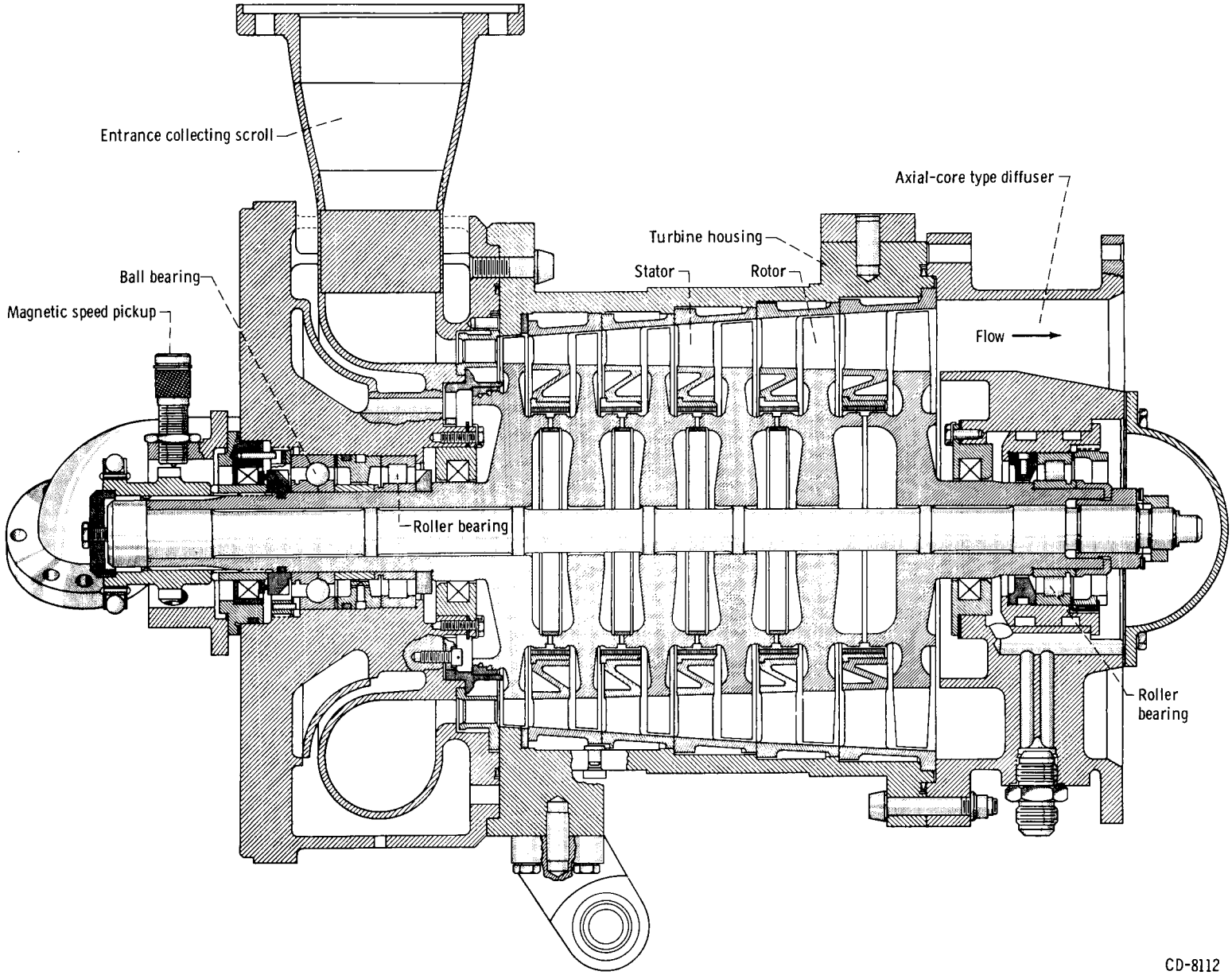

Figure 5. - Cross section of Mark-IX turbine.

TABLE III. - TURBINE STAGE GEOMETRY AND DESIGN PERFORMANCE VALUES

Turbine stage geometry	Design performance values	
Rotor blade heights, in.	0.58, for first stage rotor, to 1.35, for last stage rotor	
Rotor mean blade diameter, in.	7.92, for first stage rotor, to 8.25, for last stage rotor	
Number of blades	77 for first three rotors 57 for fourth rotor 53 for fifth rotor 49 for sixth rotor 51 for first stage nozzle row 37 for second, third, and fourth stators 41 for fifth stator 31 for sixth stator	
	Design	Hot hydrogen gas
Power parameter (at design), $HP/p_{t,0}\sqrt{RT_{t,i}}$	0.303	0.241
Pressure ratio (at design), $P_{t,i}/p_{t,0}$	12.67	11.82
Flow parameter (at design), $\dot{w}_t\sqrt{RT_{t,i}}/p_{t,0}$	133	129
Estimated efficiency, percent	68.1	57.8
Speed parameter (at design), $N\sqrt{RT_{t,i}}$	41.15	28.9

Instrumentation

The turbopump assembly was instrumented to determine the operational status of the components during the test runs and to obtain the performance data presented in this report. The operation-related instrumentation consisted of thermocouples, resistance thermometers, and accelerometers. The locations of these instruments are shown in figure 6. Operational instruments are designated by an asterisk. The performance-related instrumentation consisted of pressure transducers, a volumetric turbine flowmeter, and electromagnetic speed pickups. The locations of these instruments are also shown in figure 6. The performance-related instrumentation, although primarily used to obtain the performance data, was also used to observe the status of the turbopump in the control room during a test run.

For one of the test runs, the pump, dynamic torquemeter, and turbine rotors were locked by using a static-torque measuring device in order to obtain the pump zero-speed pressure and torque characteristics. A photograph of the device is shown in figure 7. The static-torque measuring device consisted of a 5/8-inch-square aluminum bar about 15 inches long attached to the coupling between the dynamic torquemeter and the turbine. The other end was held firm, thus allowing forces in the rotor to load the aluminum bar. There were two independent strain-gage circuits to indicate strain in the precalibrated bar. The output signal represented units of torque directly.

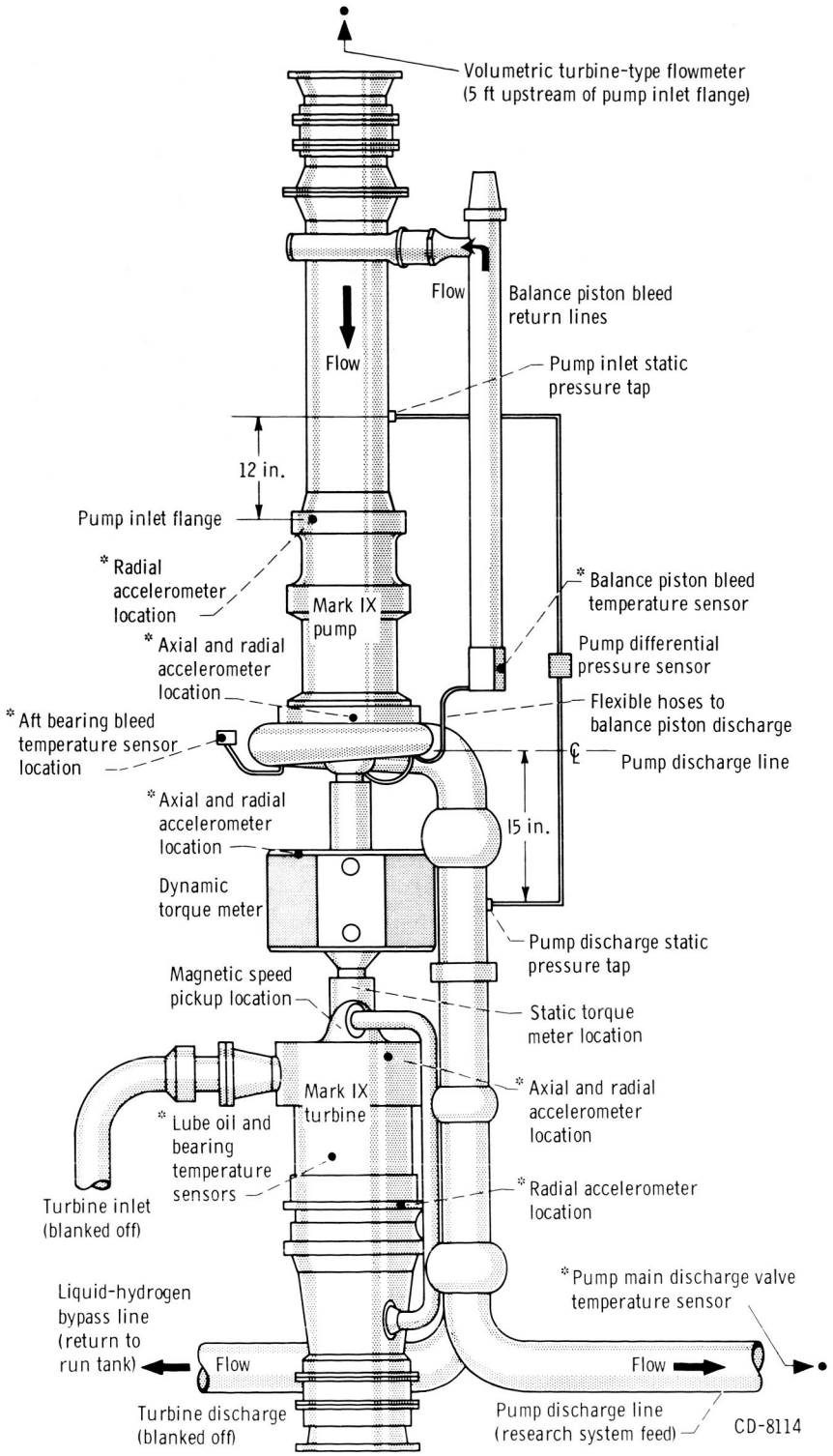

Figure 6. - Mark IX turbopump test setup with instrumentation locations.
(Asterisks denote operational instruments.)

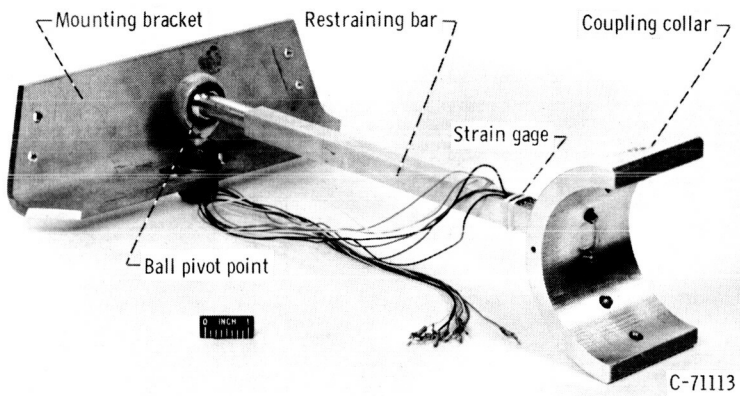

Figure 7. - Static torque measuring device.

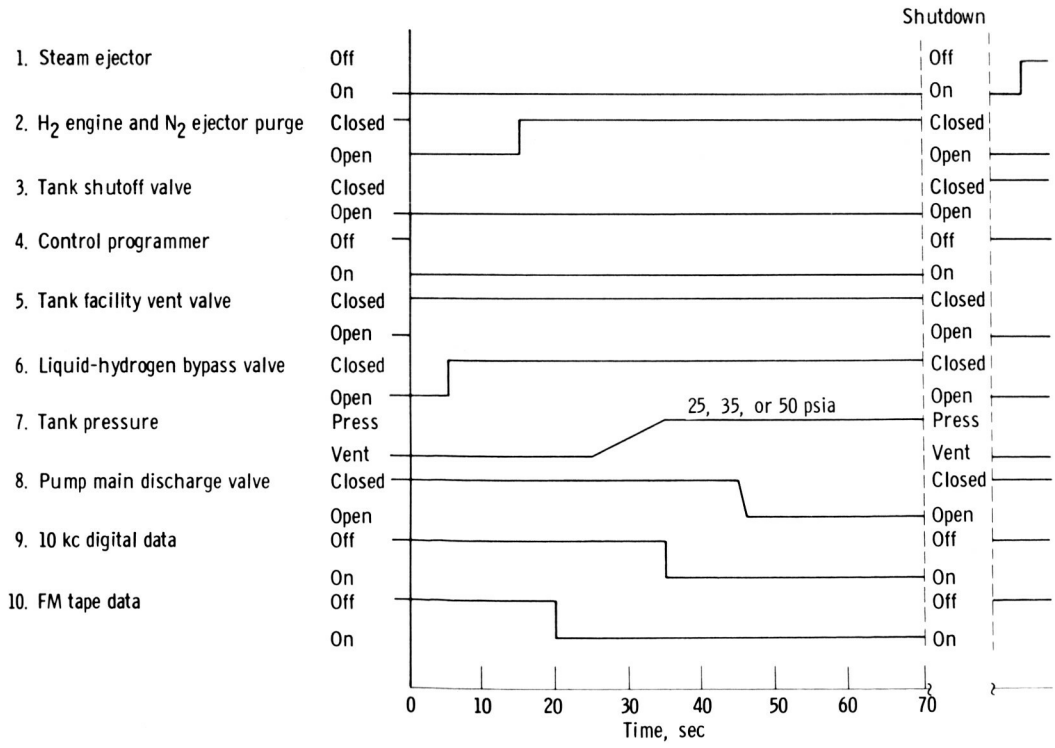

(a) Type I test.

Figure 8. - Automatic run sequence diagram.

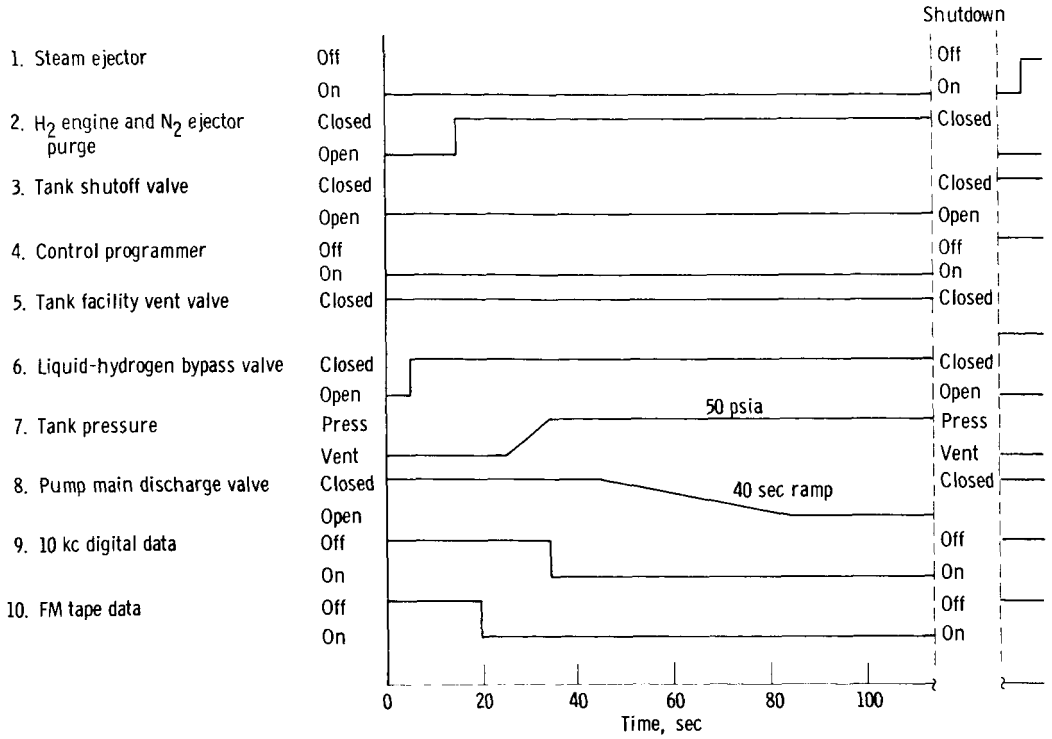

(b) Type II test.

Figure 8. - Continued.

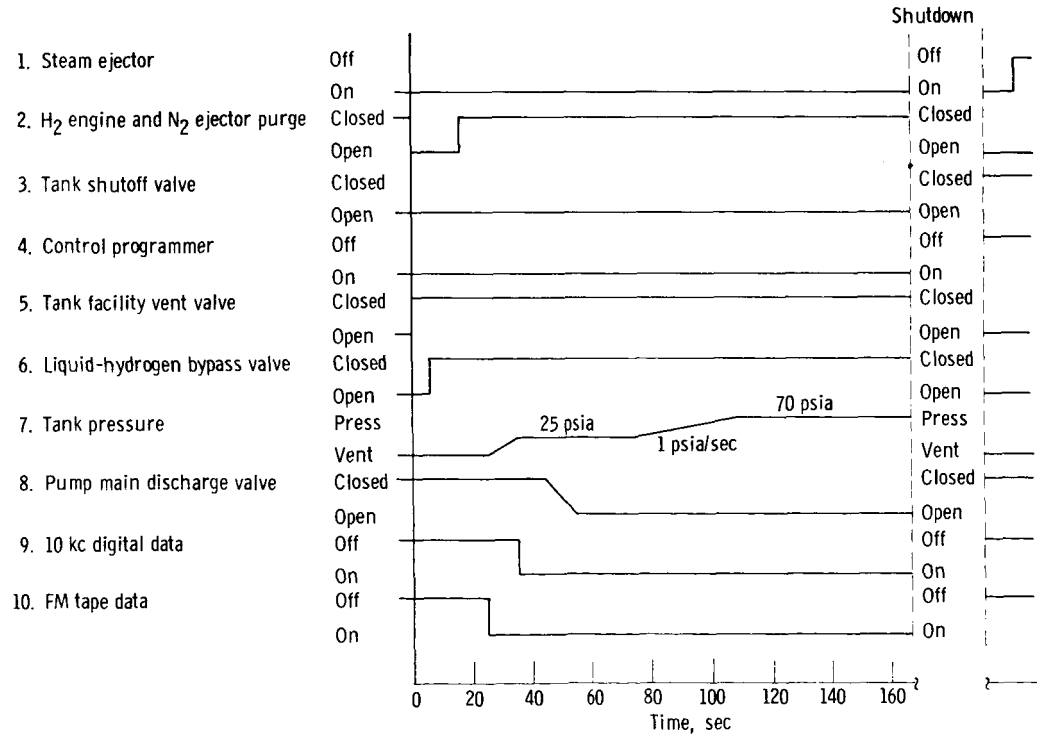

(c) Type III test, locked rotor.

Figure 8. - Concluded.

PROCEDURES

Experimental Operations

The test procedures used to produce the experimental turbopump results presented in this report were governed by the test operation of the overall research system. A brief description of this operation is given below.

The prerun procedure consists of the system cleanup (accomplished through several vacuum-evacuation and helium-purge cycles), filling the run tank, and chilldown of the pump. During the cleanup phase, the system is vented to within 1 inch of water (referenced to atmospheric conditions) and an electrical calibration of the instrumentation is taken. After the run tank is filled with liquid hydrogen, pump chilldown is begun by closing the main pump discharge valve and opening the tank shutoff and liquid-hydrogen bypass valves (see fig. 2, p. 4). The run tank is normally vented to atmosphere using a 3-pounds-per-square-inch cracking pressure vent valve during the chilldown process. Liquid-hydrogen boiloff is vented from the system using the tank vent valve and vent lines on the pump balance piston return lines and immediately upstream of the main pump discharge valve. Chilldown is considered completed when temperature sensors at the pump balance piston discharge, the aft bearing discharge, and the main pump discharge valve (see fig. 6, p. 11) indicate a stable liquid-hydrogen temperature. The time required to complete chilldown is normally from 1 to 2 hours. After chilldown is completed, the run tank is refilled to the desired run condition level.

The run procedure begins with the evacuation of the facility exhaust system using the facility steam ejectors. When the reactor nozzle exit pressure reaches 3 pounds per square inch absolute, an automatic run sequencer is initiated. The automatic sequencer produces the time sequencing of events (such as starting the data recorders and actuating the control valves) that is required to obtain the test conditions for a particular run. The time history of events, produced by the automatic run sequencer, used during the experimental investigation is shown in figure 8. Three distinct types of test runs were conducted and are shown in figure 8(a) for the Type I (free rotor, 1-sec ramp opening of the main pump discharge valve, and a constant tank pressure), figure 8(b) for the Type II (free rotor, 40-sec ramp opening of the main pump discharge valve, and a constant tank pressure), and figure 8(c) for the Type III (locked rotor, 10-sec ramp opening of the main pump discharge valve, and the tank pressure ramp from 25 to 70 psia). Only the events concerning the system operation and the acquisition of turbopump performance data are shown on these figures.

Shutdown is generally initiated using a manually activated shutdown sequencer. Automatic shutdown is also available from several safety monitoring devices including fire, hydrogen leaks, low run-tank level, and low control-valve hydraulic pressure. Upon initiation of the shutdown sequence, the liquid-hydrogen bypass and the tank-facility vent valves are opened and the tank-pressure servocontrol valves are closed. The pump-discharge valve is closed and the research and facility systems are purged with helium and nitrogen gas. Data recorders are automatically stopped and the tank shutoff valve is manually closed.

Processing of Experimental Data

The experimental data pertaining to the pump performance during the test runs was recorded on frequency modulation (FM) magnetic tape and on a 10 000-sample-per-second (10 kc) digital recording system. The FM recordings are used to observe high-frequency oscillations which pertain to dynamic conditions existing in the system while the digital recordings, although lower in frequency response, are used to obtain a more accurate reading of the absolute value of the data recorded on a given parameter. Because of the higher accuracy and since high-frequency dynamics are of minor importance in the subject investigation, the 10-kilocycle digital data were used for determining the experimental results. After the test run, the 10-kilocycle digital data were processed through an 1103 computer program which converted the sensor output signals into engineering units and applied the individual data-sensor calibrations. The computer output is a tabulation of the data at each 0.1 second during the test run. Since 100 sensor inputs are fed into the 10-kilocycle data system from the experimental research system, each point printed out represents an average of ten individual input readings. In addition to the printout of actual data, Δp and N, terminal calculations are performed in the computer to obtain the weight flow rate $\dot{w}$ from the turbine-type volumetric flowmeter output, the accelerating torque

$$M_{ACC} = -\frac{2\pi}{60} I\dot{N} \tag{1}$$

and the generalized parameters ($\Delta p/\dot{w}^2$, $N/\dot{w}$, and $M_{ACC}/\dot{w}^2$) that are presented in this report. The minus sign in equation (1) indicates that acceleration of the rotor is due to the action of the fluid. All symbols are defined in appendix A.

Estimations of data accuracies were made by utilizing the manufacturer's sensor calibrations and the inherent inaccuracies of the data acquisition and recording systems. Due to the complexity of the systems and the long transmission cabling used to send the sensor signals from the experimental system to the recording system (approx 5000 ft), a signal noise level was present on all the data channels. This error, coupled with the data acquisition system and sensor inaccuracies, results in an overall estimated error of ±1 percent of the sensor full-scale calibration value on all the data presented in this report. The estimated absolute value of error for each measured parameter (as a function of run-tank pressure used) is given in table IV.

TABLE IV. - ESTIMATED MAXIMUM INSTRUMENTATION ERRORS

Measurement	Error	Tank pressure, psia
Static pressure drop, lb/sq in.	0.10 .50	25 and 35 50 and 25 to 70
Pump flow rate, lb/sec	0.10 .25	25 and 35 50 and 25 to 70
Pump rotational speed, rev/min	10 30	25 and 35 50
Pump static torque, ft/lb	0.40	25 to 70

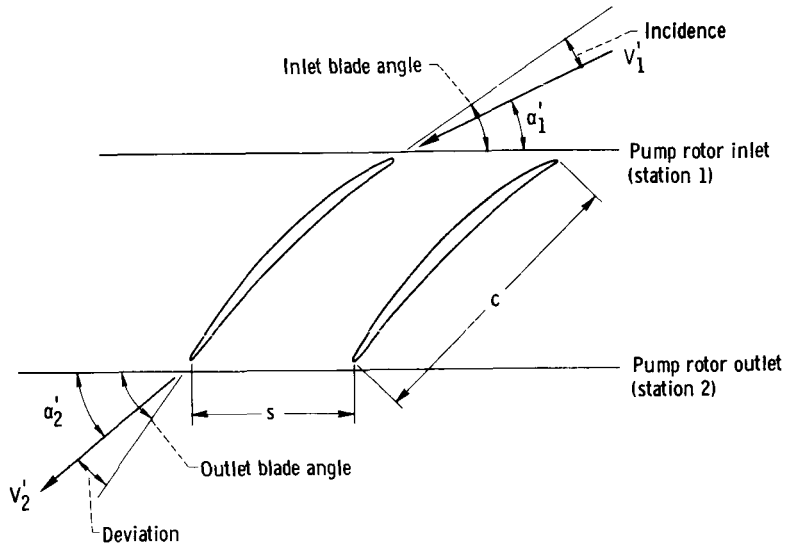

(a) Typical stage geometry.

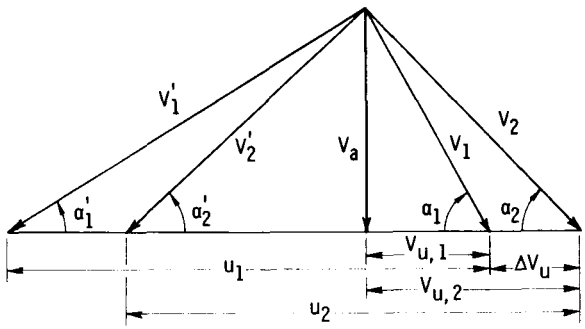

	Mean blade velocity diagrams			
	Inducer rotor		Axial stage rotor	
	Design point deviation	Zero deviation	Design point deviation	Zero deviation
Axial velocity, $V_{a,1}$, ft/sec	105		315	
$V_{a,2}$, ft/sec	309		315	
Blade velocity, u_1, ft/sec	756		985	
u_2, ft/sec	977		985	
Absolute flow angle, α_1, deg	90	90	69	78.5
α_2, deg	35.85	34.5	36.5	35.25
Relative flow angle, α_1', deg	7.9	11.6	20	20
α_2', deg	29.8	30.6	30	35.75

(b) Velocity diagram nomenclature and data of mean blade velocity diagrams.

Figure 9. - Mark IX pump stage geometry and data.

Percentage error values can be obtained for the data presented in this report by referencing the absolute error values given in table IV to the experimental time variant data plots which are presented subsequently.

Theoretical Analysis

The derivation of equations necessary for the theoretical analysis is explained in detail in appendix B and only a brief discussion of this analysis is presented at this time. A general energy equation (B1)

$$\Delta h = \frac{\Delta V^2}{2g} + \frac{g_c}{g} W + \frac{g_c}{g} \Phi \tag{B1}$$

has been written to describe the startup performance characteristics of any pump. With the aid of information presented in figure 9, equation (B1) was transformed into equation (B3) given below

$$\frac{\Delta h}{Q^2} = \left(\frac{1}{2g\Omega_1^2 \sin^2\alpha_1} \right)_{n=1} - \left[\frac{y^2}{2g\Omega_1^2 \sin^2\alpha_1} - \frac{\pi y r_2 \cos \alpha_2'}{30g\Omega_1 \sin \alpha_1} \left(\frac{N}{Q} \right) \right.$$

$$\left. + \frac{\pi^2 r_2^2}{1800g} \left(\frac{N}{Q} \right)^2 \right]_n - \sum_{j=1}^{n} \left\{ \frac{k_{f,s} + y^2 k_{f,r} + k_r^2 + y^2 k_s^2}{2g\Omega_1^2 \sin^2\alpha_1} \right.$$

$$+ \frac{\pi r_1 \left(\cos \alpha_1 + y \frac{r_2}{r_1} \cos \alpha_2' - k_r - y \frac{r_2}{r_1} k_s \right)}{30g\Omega_1 \sin \alpha_1} \left(\frac{N}{Q} \right)$$

$$\left. + \left[1 - \left(\frac{r_2}{r_1} \right)^2 \right] \frac{\pi^2 r_1^2}{1800g} \left(\frac{N}{Q} \right)^2 \right\}_j \tag{B3}$$

The work and loss terms of the energy equation (B1) are now explicit functions of the rotational speed/flow ratio N/Q, flow angles, and pump design parameters. Equation (B3) is the final expression for the windmilling characteristic. The generalized head drop parameter $\Delta h/Q^2$ and the generalized speed parameter N/Q are preferred herein rather than the more conventional head and flow parameters $\Delta h/N^2$ and Q/N because the former allow the analysis to extend to the zero speed point. (The usual flow and head parameters would both be infinity with N equal to zero.) In reference 4 both types of parameters have been used to describe operational characteristic (including windmilling) of an idealized pump operating with an incompressible, frictionless fluid.

Equation (B3) may be used in the startup analysis of any type turbopump or

hydraulic turbine. In this equation N/Q is an independent variable. In addition to pump design data, this equation contains two parameters which must be determined before any numerical calculations can be made; these are the amount of deviation on blades (to calculate α_1 and α_2'), and the amount of blockage due to the boundary layer on the walls of the annulus and blockage due to the turbulence induced by incidence (to calculate the flow area Ω_1). Because of the uncertainty of the amount of deviation in both rotor and stator blading, the equation is solved for two selected boundary conditions: that of the relative fluid outlet angles equal to the blade angles (no deviation) and the design-point outlet flow angles (design-point deviation). See figure 9(a) for deviation illustration. The flow area has been calculated using the blockage factor evaluated for the design point operation.

Besides the described head characteristic, a theoretically available fluid torque characteristic is also established. Torque of turbomachines is defined by equation (B5) as

$$M_F = \frac{\dot{w}}{g} \sum_{j=1}^{n} (r_2 V_{u,2} - r_1 V_{u,1})j \tag{B5}$$

By transformations similar to those used in the head equation, a linear equation, (eq. (B6)), relating the torque parameter $M_F/\rho Q^2$ and the speed parameter N/Q is obtained

$$\frac{M_F}{\rho Q^2} = \frac{1}{g_c} \sum_{j=1}^{n} \left(\frac{\pi r_2^2}{30} \frac{N}{Q} - \frac{r_1 \cos \alpha_1}{\Omega_1 \sin \alpha_1} - \frac{y r_2 \cos \alpha_2'}{\Omega_1 \sin \alpha_1} \right) j \tag{B6}$$

Since the fluid torque also depends on the amount of deviation, which is difficult to evaluate for the windmilling operation, again two boundary conditions have been considered and evaluated, namely that of torque resulting from flow with no deviation and torque resulting from flow with the design-point deviation.

The accelerating torque of windmilling turbomachines is defined by equation (B7):

$$M_F = M_{ACC} + M_W + M_{PL} + M_{BS} \tag{B7}$$

It is that part of the torque supplied by the fluid which serves to increase the speed of the rotor. Using the previously derived available fluid torque equation and evaluating the different resisting torques, the final expression for the accelerating torque is given by equation (B9)

$$\frac{M_{ACC}}{\rho Q^2} = \frac{1}{g} \sum_{j=1}^{n} \left[B\left(\frac{N}{Q}\right) - A \right] j + \frac{k_{BS}}{\rho Q^2} + \frac{k_W}{\rho} \left(\frac{N}{Q}\right)^2 \tag{B9}$$

RESULTS AND DISCUSSION

Theoretical Results

The theoretically derived startup characteristics will be applied to and discussed in connection with a Mark IX liquid-hydrogen turbopump whose details of construction, design data, and design-point performance are known.

Evaluation of constants and coefficients. - Information given in the APPARATUS AND INSTRUMENTATION section of this report and in figure 9 is sufficient to evaluate the pump parameters of equation (B3), namely: the rotor inlet loss coefficients k_r, the stator inlet loss coefficients k_s, the rotor frictional loss coefficients $k_{f,r}$, the stator frictional loss coefficients $k_{f,s}$, and the velocities ratios y. The flow area Ω_1, equal to the annulus area times (1 - blockage), will be calculated, for the axial stages, using the given annulus and an assumed blockage of 15 percent. For the inducer stage Ω_1 will be determined by continuity considerations with respect to the axial stages, for example, a 3 percent blockage in the inducer stage corresponds to a 15 percent blockage in the axial stages.

The resisting torque coefficients, the bearing and seals loss coefficient k_{BS}, and the windage loss coefficient k_W must be determined using experimental data for flow Q and rotational speed N. They will be established using two boundary conditions: zero accelerating torque at zero speed (when flow is Q_B), and zero accelerating torque at steady windmilling, using experimental N/Q, with the condition that k_{BS} at steady windmilling (kinetic friction condition) equals 75 percent of k_{BS} at zero speed when static friction opposes motion.

Mark IX generalized startup characteristics. - All subsequent equations will be based on 15-percent flow blockage and each characteristic will be evaluated for the design-point deviation and for the zero deviation. After the constants of equation (B3) are evaluated, the head characteristic for the design-point deviation becomes

$$\frac{\Delta h}{Q^2} = -363 + 0.346\left(\frac{N}{Q}\right) - \frac{7.75}{10^6}\left(\frac{N}{Q}\right)^2 \tag{2}$$

and for the zero deviation

$$\frac{\Delta h}{Q^2} = -300 + 0.329\left(\frac{N}{Q}\right) - \frac{7.75}{10^6}\left(\frac{N}{Q}\right)^2 \tag{3}$$

The fluid available torque characteristic (eq. (B6)) for the design-point deviation becomes

$$\frac{M_F}{\rho Q^2} = \frac{1.72}{10^3}\left(\frac{N}{Q}\right) - 1.62 \tag{4}$$

And for the zero deviation

$$\frac{M_F}{\rho Q^2} = \frac{1.72}{10^3}\left(\frac{N}{Q}\right) - 1.22 \qquad (5)$$

Making use of the preceding equations, the head parameter $\Delta h/Q^2$ and the torque parameter $M_F/\rho Q^2$ are plotted on figure 10 against the speed parameter N/Q for this turbopump, for both the zero and the design-point deviation in the flow angles.

The established head characteristics are quadratic and slightly concave downward. They tend to converge as the speed parameter increases, as shown in figure 10. Some significant points of these characteristics to be noticed are:

(1) The zero-speed point where head-drop parameter $\Delta h/Q^2$ reaches a maximum value.

(2) The zero head-drop point where the pump develops enough head to compensate for the losses.

(3) The zero-work-done point which is also the zero-torque point. At this point, which lies somewhere between the two other points, the pump has reached its windmilling equilibrium, that is, the maximum speed corresponding to the acting tank pressure.

By application of equation (B4)

$$\left(\frac{N}{Q}\right)_{\text{zero torque}} = 945 \qquad \text{for the design-point deviation}$$

and

$$\left(\frac{N}{Q}\right)_{\text{zero torque}} = 712 \qquad \text{for the zero deviation}$$

The zero-torque point divides the head-drop characteristic into two parts. From $N/Q = 0$ to the N/Q corresponding to zero torque, the characteristic pertains to accelerating windmilling. The other part of the Δh characteristic line, up to the axis, is that portion of the characteristic where the pump internal-flow losses exceed the turbine energy supply. The two linear characteristics (M/Q^2, on fig. 10), are the available fluid torque functions calculated by equation (B6) and for 15 percent blockage in the axial stages. The design-point deviation (lower line) and zero deviation (upper line) characteristics are shown. The two lines indicate zero torque at speed parameters N/Q equal to 945 and 712 respectively, as established using the head equation.

The two zero-torque points determine, besides two N/Q values, two $\Delta h/Q^2$ values. The head-drop parameter $\Delta h/Q^2$ at zero torque fixes the head loss Δh that is required to assure steady windmilling of the pump when the flow Q is available.

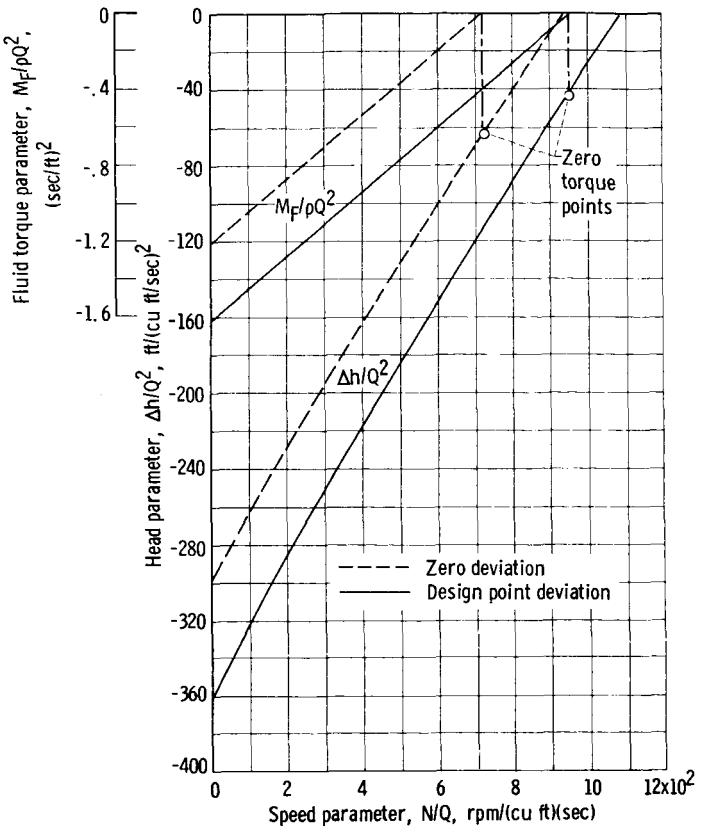

Figure 10. - Generalized flow and available torque theoretical characteristics.

The influence of blockage on the characteristic is shown in figure 11. A blockage of 15 percent in the axial stages is used in the present study. A 20-percent blockage results in losses 20-percent higher, on the average.

Mark IX startup characteristics - liquid hydrogen flow. - The generalized characteristics may be recalculated in dimensional form to allow comparison with data. For a constant liquid hydrogen density of 4.4 pounds per cubic foot (assuming tank temperature constant) $Q = \dot{w}/\rho = \dot{w}/4.4$ and $\Delta h = 32.7\ \Delta p$, the pressure drop and the fluid-torque characteristics of the pump startup with liquid hydrogen using equations (2) to (5) are as follows:

The pressure characteristic for the design-point deviation is

$$\frac{\Delta p}{\dot{w}^2} = -0.575 + \frac{2.40}{10^3}\left(\frac{N}{\dot{w}}\right) - \frac{0.237}{10^6}\left(\frac{N}{\dot{w}}\right)^2 \qquad (6)$$

and for zero deviation

$$\frac{\Delta p}{\dot{w}^2} = -0.473 + \frac{2.29}{10^3}\left(\frac{N}{\dot{w}}\right) - \frac{0.237}{10^6}\left(\frac{N}{\dot{w}}\right)^2 \qquad (7)$$

The available fluid torque characteristic for the design-point deviation is

$$\frac{M_F}{\dot{w}^2} = \frac{1.72}{10^3}\left(\frac{N}{\dot{w}}\right) - 0.370 \qquad (8)$$

and for zero deviation

$$\frac{M_F}{\dot{w}^2} = \frac{1.72}{10^3}\left(\frac{N}{\dot{w}}\right) - 0.279 \qquad (9)$$

Using equation (B9) and equation (8) the accelerating-torque characteristic for the design-point deviation becomes

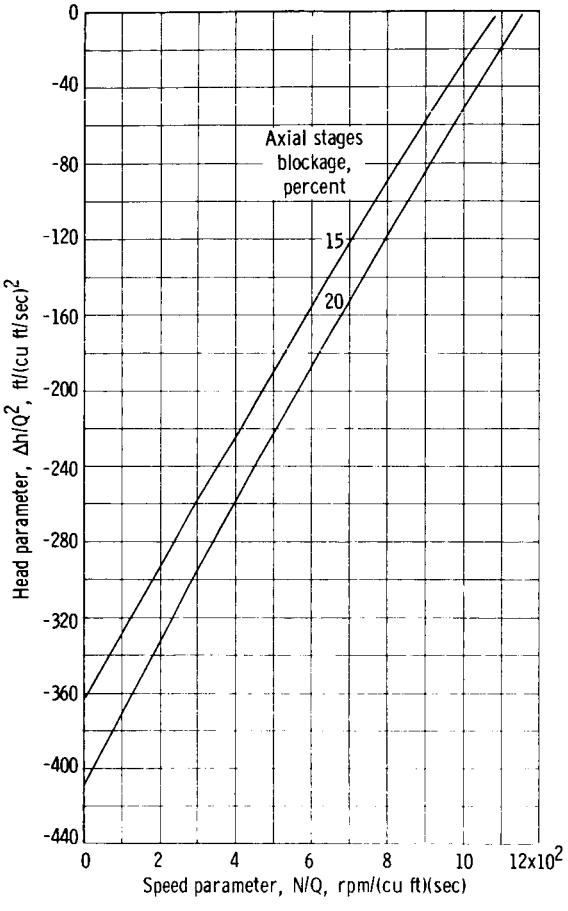

Figure 11. - Influence of blockage on flow theoretical characteristic.

$$\frac{M_{ACC}}{\dot{w}^2} = \frac{1.72}{10^3}\left(\frac{N}{\dot{w}}\right) - 0.370 + \frac{k_{BS}}{\dot{w}^2} + k_W\left(\frac{N}{\dot{w}}\right)^2 \qquad (10)$$

The established characteristics (eqs. (6) to (10)) will be shown subsequently when test data will be compared with theoretical results.

Mark IX startup characteristics - liquid-nitrogen flow. - Using a liquid-nitrogen density of $\rho = 50.4$ pounds per cubic feet, the pressure drop and the fluid torque characteristics of pump startup with liquid nitrogen, as defined by equations (2) to (5), are as follows:

The pressure characteristic for the design-point deviation is

$$\frac{\Delta p}{\dot{w}^2} = -0.0500 + \frac{2.40}{10^3}\left(\frac{N}{\dot{w}}\right) - \frac{2.71}{10^6}\left(\frac{N}{\dot{w}}\right)^2 \qquad (11)$$

and for the zero deviation

$$\frac{\Delta p}{\dot{w}^2} = -0.0412 + \frac{2.29}{10^3}\left(\frac{N}{\dot{w}}\right) - \frac{2.71}{10^6}\left(\frac{N}{\dot{w}}\right)^2 \qquad (12)$$

The available fluid torque characteristic for the design-point deviation is

$$\frac{M_F}{\dot{w}^2} = \frac{1.72}{10^3}\left(\frac{N}{\dot{w}}\right) - 0.0323 \qquad (13)$$

and for zero deviation

$$\frac{M_F}{\dot{w}^2} = \frac{1.72}{10^3}\left(\frac{N}{\dot{w}}\right) - 0.0243 \qquad (14)$$

The four theoretical characteristics (eqs. 11 to 14) will be shown in connection with the evaluation of test data and comparison with theoretical results.

Experimental Results

The experimental results obtained from the three types of test runs con-

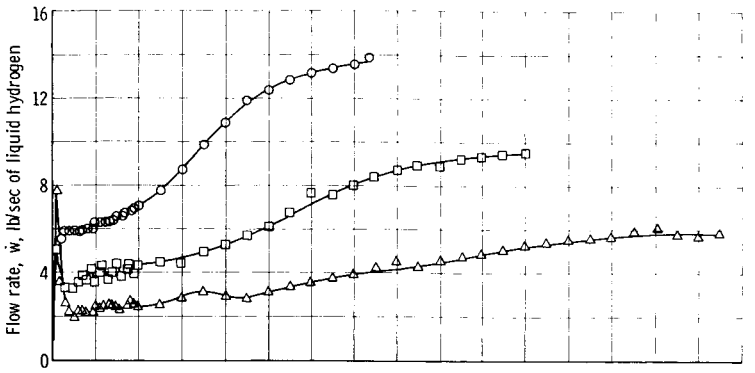

(a) Flow rate against time.

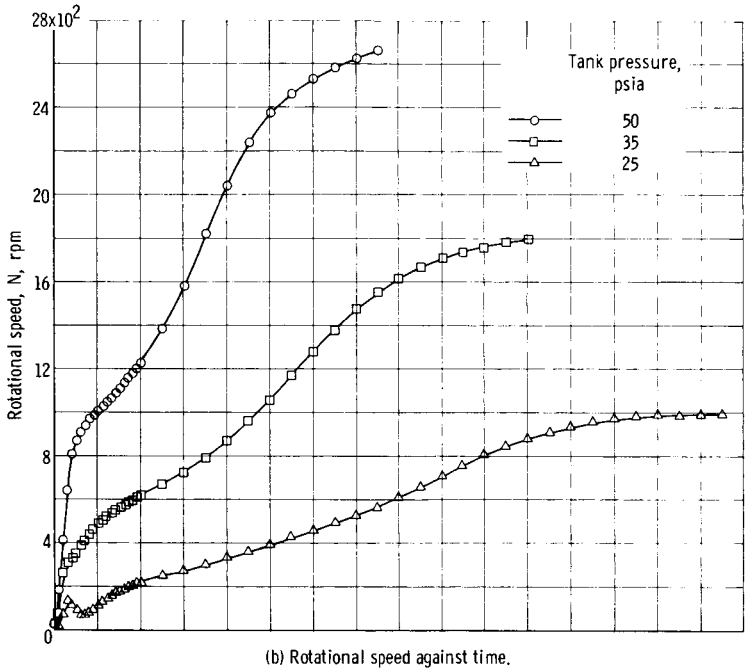

(b) Rotational speed against time.

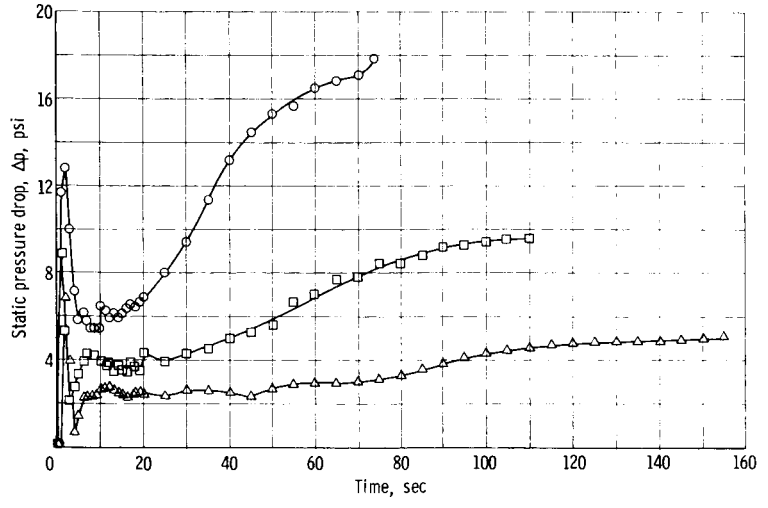

(c) Static pressure drop against time.

Figure 12. - Experimental performance characteristics of Mark IX turbopump for Type I tests.

ducted (see PROCEDURES) are presented in figures 12 to 15. The variations of the measured parameters as a function of run time are presented in figures 12 to 14 and the variations in rotational speed as a function of flow rate are presented in figure 15. All of the time-history variations presented were constructed from the 10-kilocycle digital data using varying incremental time periods depending upon the degree of variation observed in each parameter. For example, the variations shown for the early portion of each run (conditions changing rapidly) were constructed using time increments of 1 second whereas during the latter portion of each run (conditions changing slowly) time increments of 5 seconds were used.

The flow-rate variations obtained from the Type I tests (free rotor, constant tank pressure, and a fast (1 sec) ramp opening of the pump main-discharge valve) are shown in figure 12(a) as a function of run time for three levels of tank pressure, 50, 35, and 25 pounds per square inch absolute. The rapid increase and subsequent oscillations noted during the initial phases of the test runs are the result of "dumping" the liquid hydrogen into the warm, evacuated system (two-phase flow). The flow-rate variations following the initial increase are the result of the changing system resistance. The rotational-speed variations which resulted from the flow rate through the pump are shown as a function of run time in figure 12(b). The resultant speed variations indicate that the large flow-rate oscillations obtained during the early portions of the 25- and 35-pounds-per-square-inch-absolute test runs had a significant influence on the turbopump acceleration. Discontinuities in the slope of the speed curves can be observed during the first 10 seconds of these two runs with an actual deceleration occurring during the 25-pounds-per-square-inch-absolute run. The deceleration in rotational speed for the 25 pounds per square inch run is attributed to the extremely large flow rate pulse (relative to the initial stabilized value) that was realized. The variations in pump static pressure drop that were obtained are presented as a function of time in figure 12(c). Oscillations in the static pressure drop were prevalent during the early portion of the runs for all the tank pressures. The flow rate and static-pressure drop oscillations that were obtained during the early portions of these runs did not allow the determination of these parameters at the pump breakaway (beginning of rotation) point.

In order to determine the pump and system reaction to a slower rate of flow initiation, a test run was conducted using a slow (40 sec) ramp opening of the main pump discharge valve and a 50 pounds per square inch absolute tank pressure (Type II test). The flow-rate variation that was obtained is presented as a function of run time in figure 13(a) and the resultant variation in turbopump rotational speed is presented as a function of run time in figure 13(b). As a result of the comparatively slow rate of change in flow rate with time and the elimination of the large initial flow-rate oscillations (25 and 35 psia tank pressure Type I tests), the flow rate required to induce turbopump rotation (breakaway) was determined. Comparison of times in figures 13(a) and (b) indicates that breakaway was realized at a flow rate of 2 pounds per second. The pump static pressure drop corresponding to breakaway was not obtained due to a malfunction in instrumentation.

To define the pump zero-speed performance, a test run was conducted with a locked pump rotor (Type III test). The pump rotor was locked using a torque-

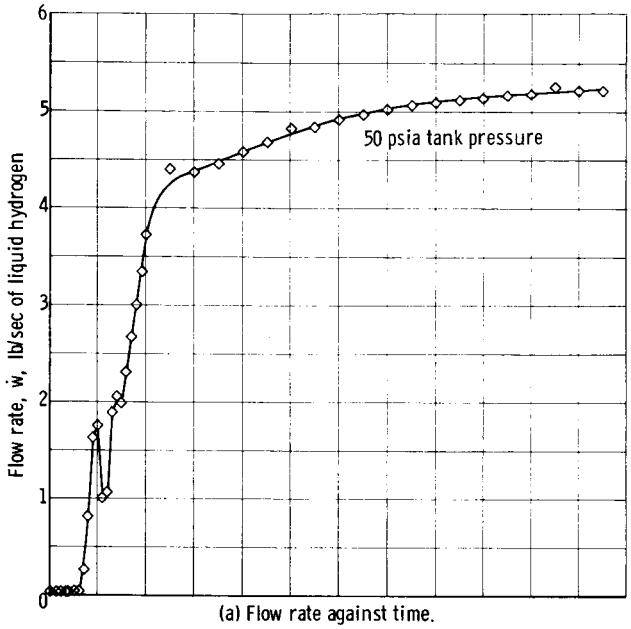

(a) Flow rate against time.

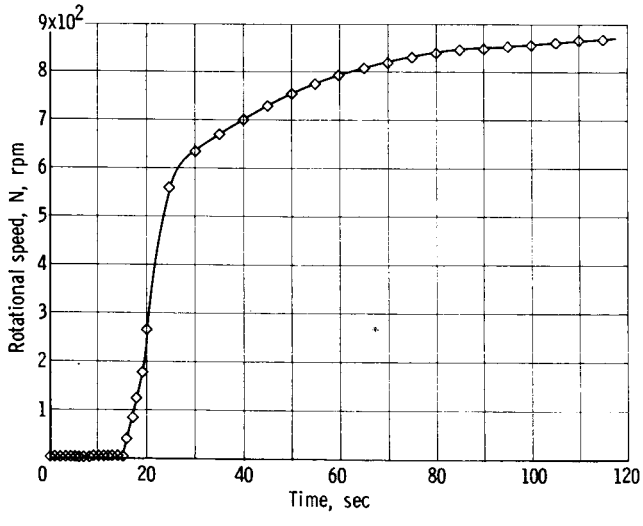

(b) Rotational speed against time.

Figure 13. - Experimental performance characteristics of Mark IX turbopump for Type II tests.

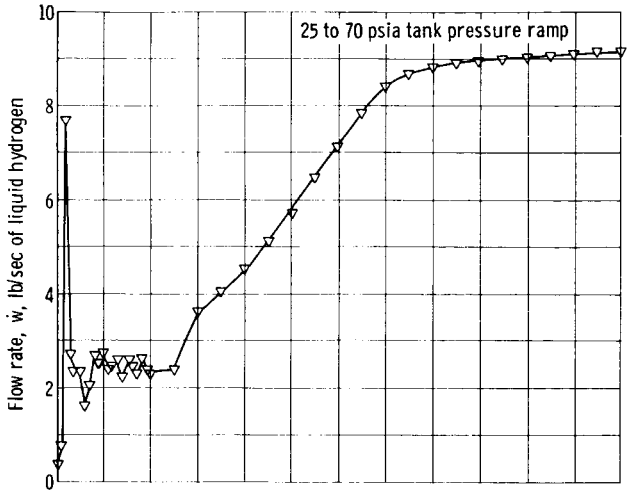

(a) Flow rate against time.

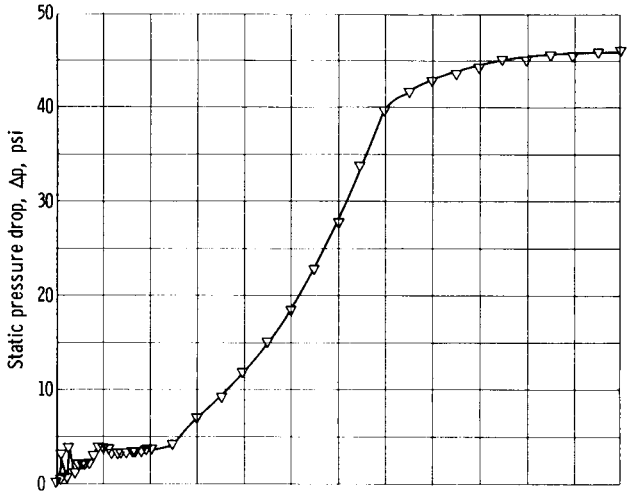

(b) Static pressure drop against time.

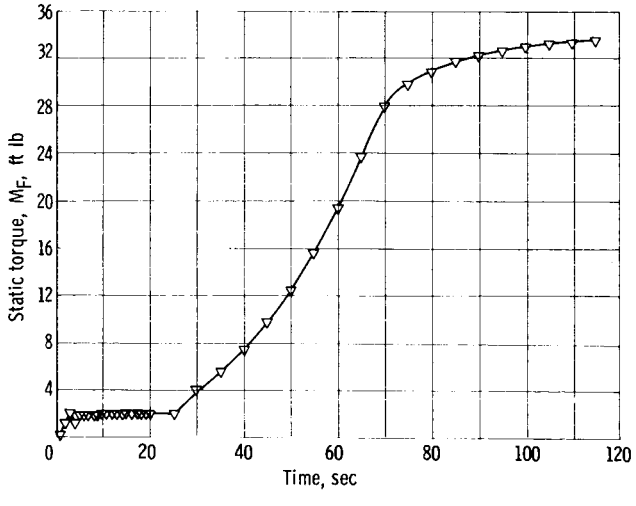

(c) Shaft torque against time.

Figure 14. - Experimental performance characteristics of Mark IX turbopump for Type III tests.

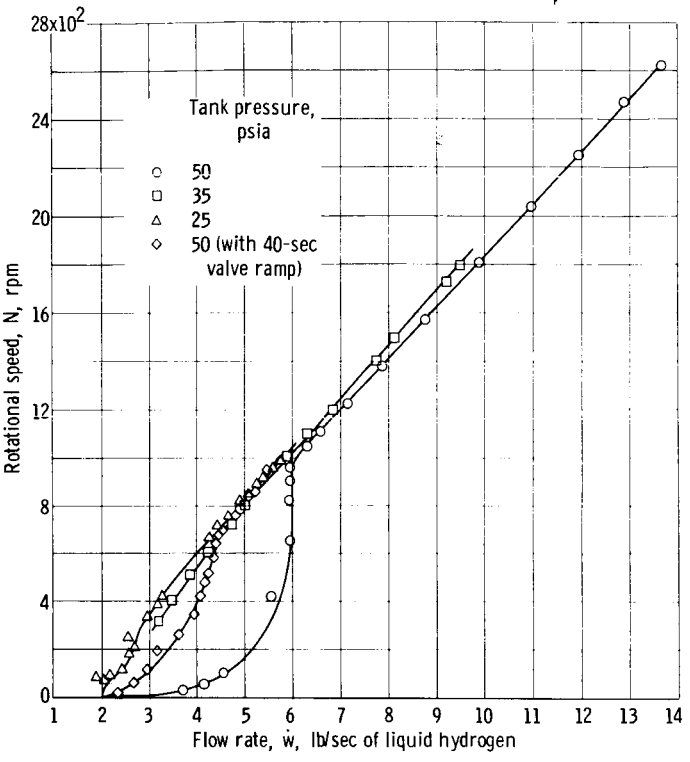

Figure 15. - Variation in rotational speed as function of flow rate.

measuring device described in the APPARATUS AND INSTRUMENTATION section of this report. The variations of the flow rate, static-pressure drop, and measured shaft torque that were obtained are shown in figures 14(a), (b), and (c), respectively. After the oscillations subsided and rapid transients were completed, the zero-speed static-pressure drop and measured torque were computed (from the data plotted on the figures) to be a constant times the flow rate squared. The computed values are: $\Delta p = 0.575\ \dot{w}^2$ and $M_F = 0.37\ \dot{w}^2$. Substituting the 2 pounds per second flow rate required for breakaway, the static pressure drop at breakaway is 2.3 pounds per square inch and the measured shaft torque is 1.48 foot-pounds. These values define the breakaway conditions of the Mark IX turbopump used in this investigation. The computed value of shaft torque gives an indication of the power that would be required to rotate the pump from a zero speed condition, with no induced flow rate and when completely filled with liquid hydrogen. The actual value of the measured torque may be somewhat in error due to undefined effects of the bearing and seal static friction on the measured value. However, for estimating purposes, the calculated value should be a good approximation.

After turbopump breakaway has been achieved in a nuclear engine startup cycle, the defining of the turbopump performance at the point at which power is first applied (beginning of bootstrapping) is also required. One possible method of startup is a preprogramed speed ramp for which the initial speed of the unit must be known. To illustrate the variation of turbopump rotational speed as a function of flow rate through the pump, data from all the test runs previously discussed are presented in figure 15. Observation of this figure indicates that a lag in turbopump rotational speed was experienced during the low flow-rate portion of all the test runs. This lag indicates a nonequilibrium between speed and flow that is caused by the fluid energy overcoming the inertia of the turbopump. The lag appears to be a function of the initial flow-rate level, the ramp opening rate of the pump discharge valve, and the time required to reach the initial (nonoscillating) flow-rate level. The definition of this lag, through experimentations such as reported herein, is necessary in order to have prior knowledge of turbopump starting conditions if a sensible and accurate engine startup cycle is to be achieved. A considerable error in initial rotational speed conditions would be obtained if the assumption was used that speed varies linearly with flow rate (normally assumed characteristic) in the low flow-rate region. After the lag is overcome and quasi-equilibrium conditions

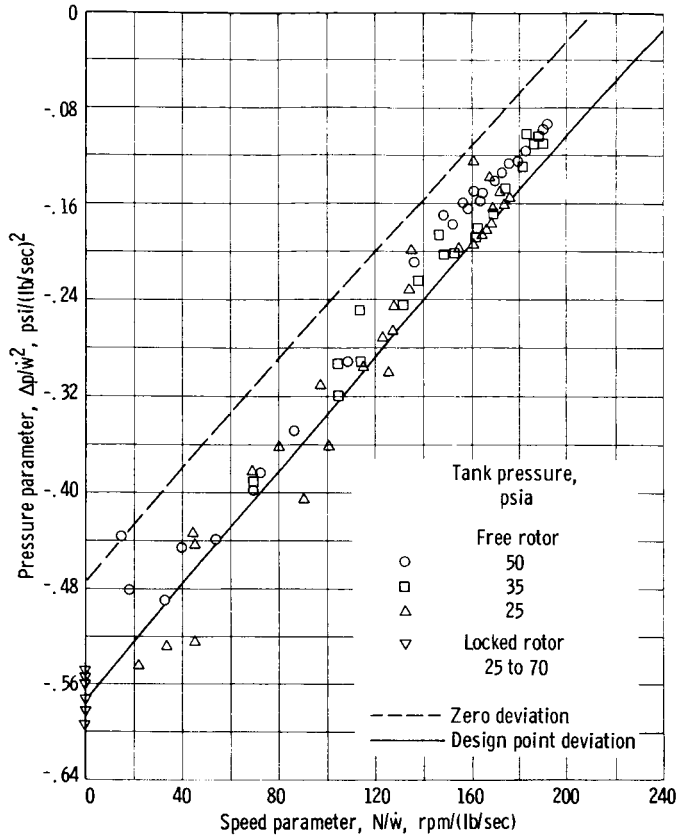

Figure 16. - Verification of analytically established flow characteristic (liquid-hydrogen runs).

are obtained, the assumption that speed varies linearly with flow rate is shown to be a fair approximation by the data plotted for the higher flow rates. Extrapolation of all the data shown in figure 15 indicates a convergence at a flow rate of 2 pounds per second, thus confirming a breakaway flow rate previously discussed.

The experimental data which are presented and discussed define the zero speed, breakaway, transient (nonequilibrium), and steady (quasi-equilibrium) performance of the Mark IX turbopump unit used in this investigation. These data, in particular the accelerating characteristics, are applicable only to the particular unit used. However, the fluid flow characteristics should be representative of all Mark IX pumps with the same blading configuration.

Experimental data obtained during two liquid-nitrogen runs conducted during the checkout of the system are not presented even though they are discussed in the comparison of results to follow.

Comparison of Theoretical and Experimental Results

The validity of the developed equations and assumptions is demonstrated in figures 16 to 21, where calculated speed, pressure, and torque parameters are plotted for both liquid hydrogen and liquid nitrogen.

Liquid-hydrogen runs. - Generalized results of four liquid-hydrogen runs previously discussed are shown in figure 16, where the time enters implicitly only. Low values of the speed parameter $N/\dot{w}$ correspond to the early moments of runs. A speed parameter $N/\dot{w}$ close to 130 was usually attained in the first 10 seconds of run. During those 10 seconds, the flow conditions were unstable and resulted in strong oscillations. $N/\dot{w}$ greater than 130 pertained to relatively uniform flow conditions. The pressure parameter against speed parameter shows a pronounced scatter with the low values of the $N/\dot{w}$ parameter, but data are well repeatable in the vicinity of steady windmilling. Generally $N/\dot{w}$ was increased with time but the rate of change was essentially nonlinear.

In figure 16, the experimental pressure parameter data are compared with theoretically predicted characteristics calculated using equations (6) and (7).

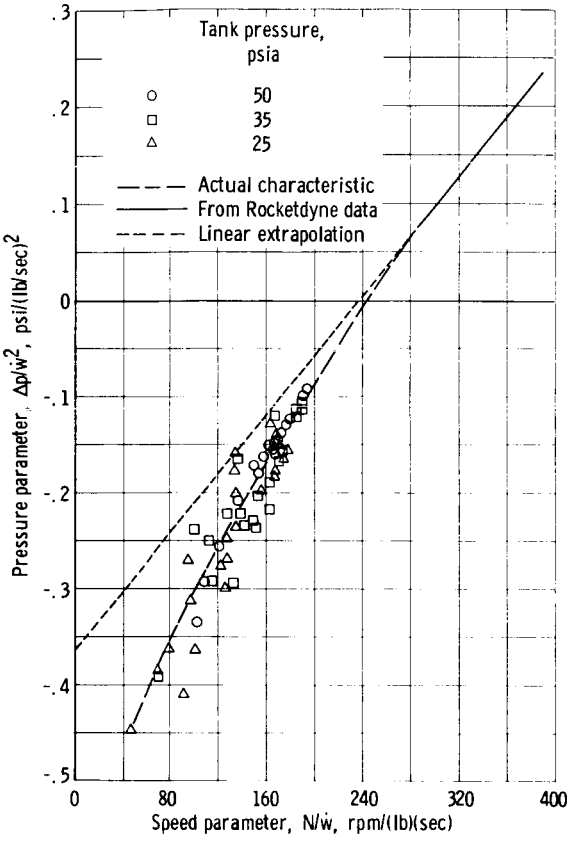

Figure 17. - Correlation between design pump characteristic and startup characteristic (liquid-hydrogen runs).

Generally, the experimental data up to $N/\dot{w} = 100$ straddle the design-point deviation line. For values of the speed parameter $N/\dot{w}$ higher than 100 the experimental data lie on and above the design point deviation line. Generally, however, the experimental data appear to lie on a steeper characteristic than predicted by the theory. This is attributed to the variation in blockage, with incidence and flow Reynolds number.

In figure 17 the results of all tests are reproduced along with a linear extrapolation of high-speed pump data. Inspection of the extrapolated line and test data suggests that, in general, the pressure characteristic of startup is approximated by a slightly curved line, rather than the linear extrapolation, which roughly may be drawn as an extension of the pump characteristic, down to near $N/\dot{w} = 0$ value.

An evaluation of the approximate location of the zero-speed torque point can be done by a similar nonlinear extrapolation.

Further useful analysis can be based on figure 18 where absolute values of pump pressure drops have been plotted against the flow rate. Data from the windmilling tests start with a flow rate of about 2 pounds per second which corresponds to the breakaway point. At low flows the strong changes of pressure drop with increasing flow pertain to the first few seconds of the runs when the inertia of the rotor produced transients in the flow characteristic. At higher flows these effects vanished and there was an almost linear variation of pressure drop with flow until the pump finally reached a steady windmilling condition.

Two limiting characteristics, each for the zero deviation and the design-point deviation, are shown in figure 18: the characteristics derived from equations (6) and (7), corresponding to flow with a locked rotor (zero speed point), and the characteristics corresponding to the zero-torque point previously discussed, derived from the same equations using $N/\dot{w}$ values obtained from equations (8) and (9).

The initial transient Δp was, at first, following the zero-speed characteristic and then abruptly would switch to a linear variation approaching the zero-torque characteristic.

The run with the locked rotor produced data which almost coincide with the zero-speed line characteristic based on the design-point deviation.

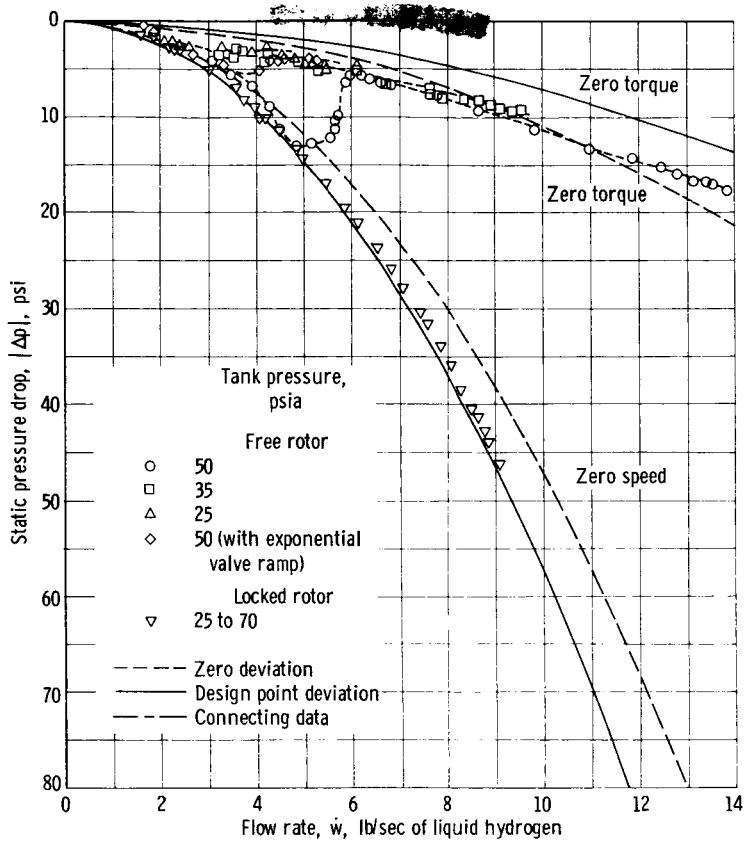

Figure 18. - Zero speed (locked rotor) and zero torque (steady windmilling) theoretical lines and corresponding test data.

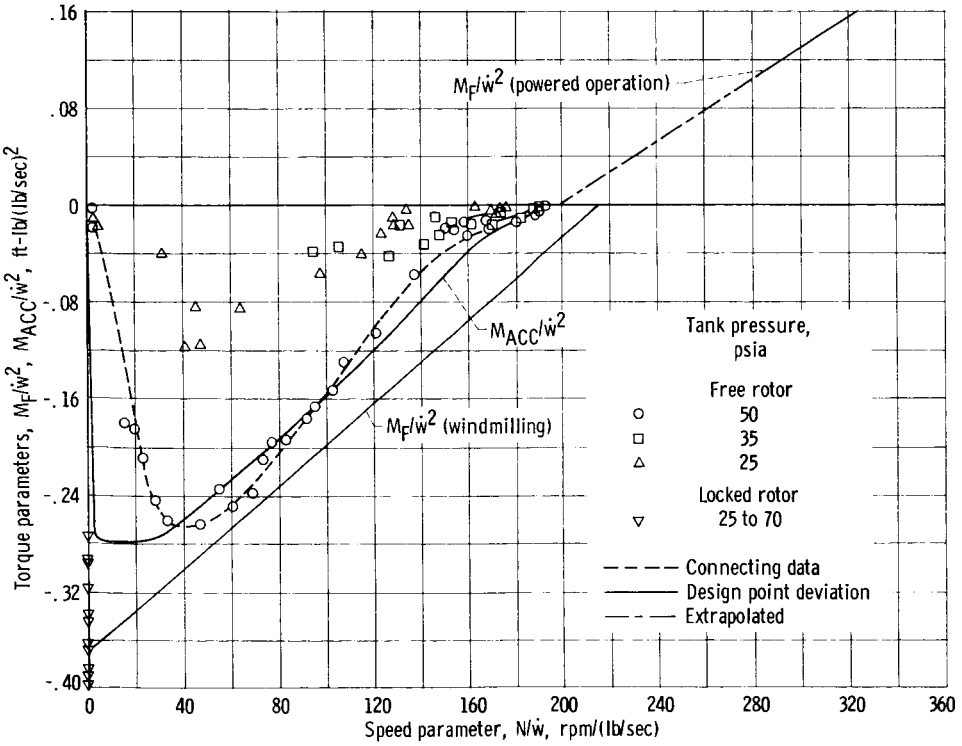

Figure 19. - Fluid torque characteristic and comparison of theoretical and test accelerating torque data for liquid hydrogen.

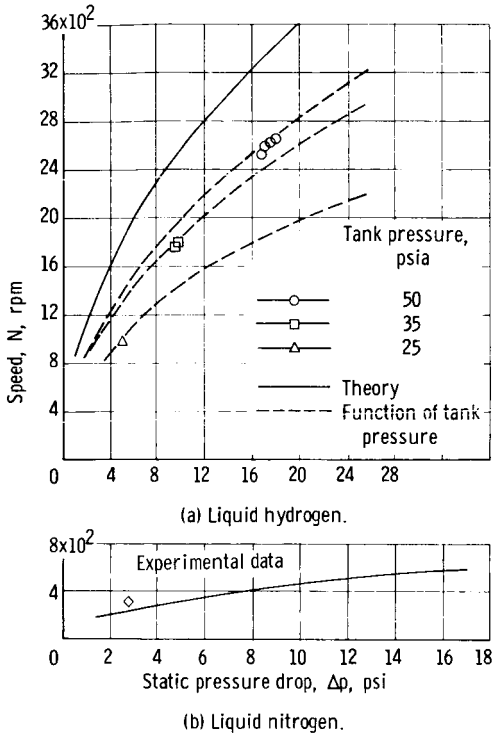

(a) Liquid hydrogen.

(b) Liquid nitrogen.

Figure 20. - Evaluation of steady windmilling (zero torque) speed and pressure drop.

The related but separate problem area, illustrated in figure 19, is the pump torque characteristics under the windmilling condition. The available fluid-torque characteristic during windmilling (by definition negative) is described by linear equations (8) and (9). By its very nature, the available fluid torque will always be affected by resisting torques, such as bearing and seal friction torque, and cannot be checked by experiment. Even in the case of no rotation, the static bearing friction will make the experimental torque reading incorrect by a constant. The torque characteristic shown in the upper part of figure 19 pertains to Mark IX operation as a pump (positive torque). The positive (experimental) and the negative (analytical) torque characteristics are discontinuous at a value of torque parameter equal to zero. In addition the slopes of the two characteristics are also discontinuous at this value of torque parameter. The discontinuity in the torque characteristic curve is due to the fact that during windmilling both deviation and probably blockage were not exactly as assumed (deviation equal to the design-point deviation and a blockage of 15 percent). The discontinuous slope is due, in part, to the variation in efficiency (not accounted for) during powered operation.

The accelerating-torque characteristic as described by equation (B10) has been calculated using test data to evaluate the terms pertaining to frictional and windage losses and is shown on the same figure. Only one full characteristic is shown because of lack of satisfactory data in the early seconds of all runs, except for the 50-pounds-per-square-inch-absolute run.

The experimental data points pertaining to the accelerating torque have been calculated by equation (1) with $\dot{N}$ taken from test data. Generally, there is satisfactory agreement between test and theory. Large transients in the first few seconds of this run cause some discrepancy between the calculated characteristics of the accelerating torque and the test data.

Comparing the fluid available torque during windmilling with the accelerating torque, figure 19, for the three free-rotor runs, it can be noticed that for a single (calculated) value of $N/\dot{w}$ corresponding to zero available torque there are three values of experimental $N/\dot{w}$ at three different tank pressures, that is, the zero accelerating torque point depends on the tank pressure. The calculated value of $N/\dot{w} = 215$ was attained within 12 percent ($N/\dot{w} = 192$) when tank pressure was 50 pounds per square inch absolute. When the pressure was 35 and 25 pounds per square inch absolute, the speed parameter reached was 190 and 175 respectively. Losses make it impossible for the pump to reach high-speed windmilling, and the lower the tank pressure (flow rate) the more

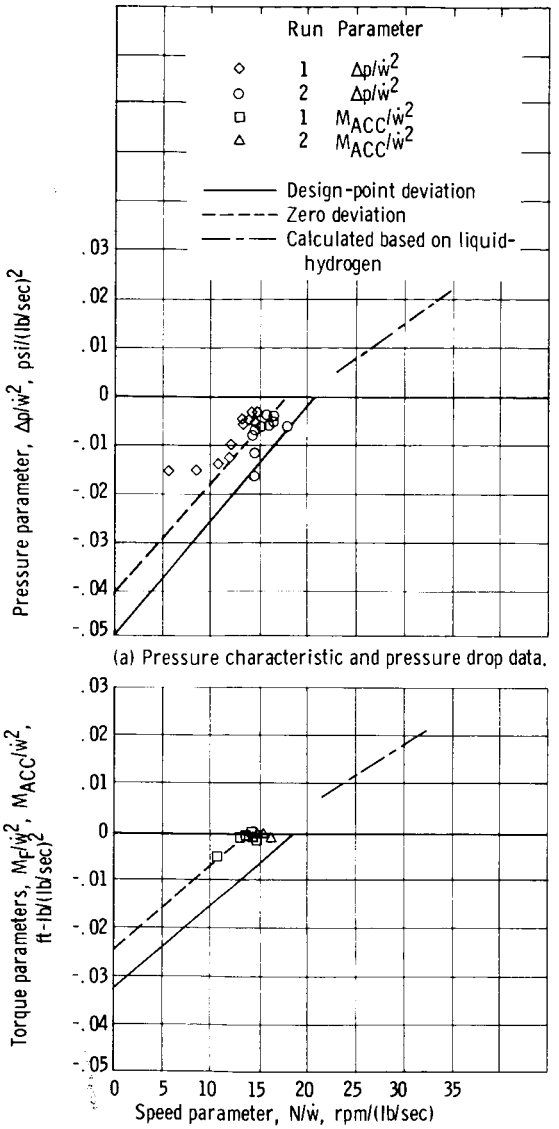

(a) Pressure characteristic and pressure drop data.

(b) Fluid torque characteristic and accelerating torque data.

Figure 21. - Verification of analytically established performance characteristics. Correlation between design pump characteristic and startup characteristic (liquid-nitrogen runs).

pronounced is this effect. This is best illustrated in figure 20(a) where an attempt is made to obtain numbers pertaining to steady windmilling. The line representing liquid-hydrogen steady windmilling speed against pressure drop across the pump (theoretical) was obtained by elimination of mass flow $\dot{w}$ between the $N/\dot{w} = 215$ and the corresponding $\Delta p/\dot{w}^2 = 0.070$ calculated by equation (6). The line is rapidly rising, indicating that windmilling strongly depends on tank pressure. The three experimental data sets of steady windmilling, produce similar characteristics and confirm the analytical evaluation but the agreement is not too good because of the resisting torque effects. A generalized expression for this type of characteristic is

$$\Delta p = \lambda \times 10^{-5} N^2$$

where, in this particular case,

$$\lambda = 0.151 + \frac{14.6}{p_T} - \frac{826}{p_T^2} + \frac{17100}{p_T^3}$$

The theoretical line does not consider any resisting torques and hence corresponds to an assumption that p_T equals infinity.

Liquid-nitrogen runs. - Figure 21(a) shows that the steady windmilling resulted in repeatable data points, which, however, lie in the higher $N/\dot{w}$ region than expected (6 percent off). Moreover, the data lie on the "zero deviation" line calculated by equation (12). Because of very low rotational speed (extreme off-design operating condition) this phenomenon is attributed to lack of deviation rather than to an effect of blockage decrease. At low Reynolds numbers blockage would probably be higher than the estimated 15 percent of the flow area.

The available accelerating torque, figure 21(b), data closely resemble the pattern of liquid-hydrogen runs. Because of the lack of data, no theoretical accelerating torque has been calculated. In figure 20(b) the pump's steady windmilling speed is plotted against pressure drop across the pump. The characteristic is calculated using $N/\dot{w} = 14.1$ and the corresponding $\Delta p/\dot{w}^2 = 0.0093$ (the steady windmilling values of parameters calculated using eqs. (12)

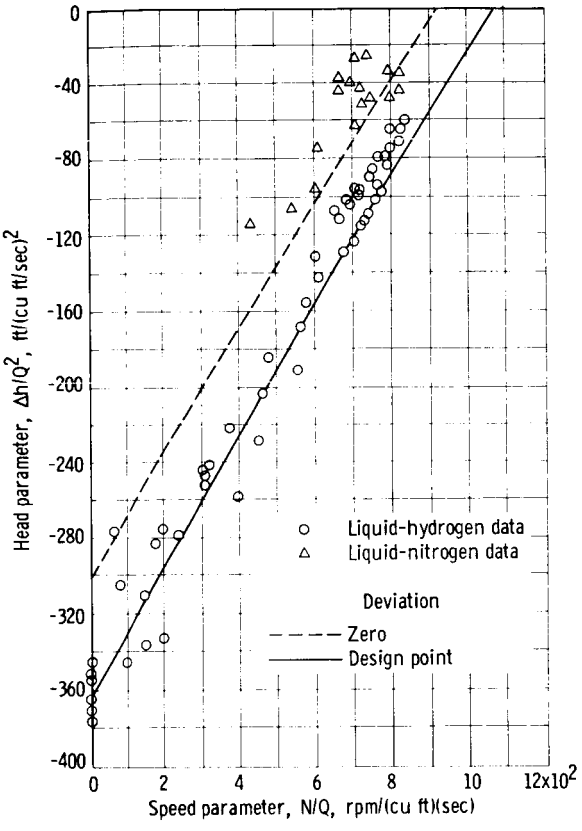

Figure 22. - Correlation of liquid-hydrogen and liquid-nitrogen test data using generalized parameters.

and (14)) and eliminating $\dot{w}$ between these two equations. The resulting equation is $\Delta p = 4.67 \times 10^{-5} N^2$. The experimental point of steady windmilling with liquid nitrogen is located slightly above the calculated curve. The low slope of the curve indicates that the steady windmilling speed that the pump may eventually reach will always remain low.

Correlation of liquid-hydrogen and liquid-nitrogen test data. - The generalized pump parameters $\Delta h/Q^2$ and N/Q along with the generalized startup characteristics, equations (2) and (3), allow a useful correlation of test data. The recalculated data points of the liquid-hydrogen and the liquid-nitrogen runs are plotted on a single diagram, figure 22.

The two boundary conditions; namely, the design-point deviation line and the zero deviations line, appear to define, with fair accuracy, the area of startup performance for a very wide range of experimental conditions.

SUMMARY OF RESULTS

The analytical and experimental investigations of the startup (zero speed, breakaway, and windmilling) performance of an axial-flow pump, installed in a nuclear rocket cold-flow system, yielded the following principal results:

1. A one dimensional hydraulic turbomachinery theory can be used to describe the startup performance of a multistage axial-flow liquid-hydrogen pump.

2. An approximate startup characteristic, expressed in terms of speed $N/\dot{w}$ and pressure $\Delta p/\dot{w}^2$ parameters, can be obtained by a nonlinear extrapolation of conventional (high-speed) pump data. The degree of nonlinearity required for this extrapolation can be estimated based on the slight curvature of the conventional pump characteristic curve. The zero-speed torque point can also be estimated using a similar extrapolation.

3. Turbopump behavior is significantly affected by the transients in the system downstream of the pump.

4. The assumption that rotational speed varies linearly with flow rate is not valid during the very early portion of inducing flow into the system. This assumption is valid after the initial rotational speed lag caused by nonequilib-

rium in overcoming the static friction and inertia of the machine has been dispelled.

5. The breakaway and accelerating performance obtained are directly applicable only to the Mark IX turbopump used in the experiment. However, this performance should be descriptive of similar Mark IX turbopumps and the fluid torque and pressure characteristics should be descriptive of axial-flow pumps having similar type blading.

Lewis Research Center,
National Aeronautics and Space Administration,
Cleveland, Ohio, July 7, 1965.

[redacted]

APPENDIX A

SYMBOLS

[Symbol lb is used for both pound force and pound mass.]

A	a parameter, $(r_1 \cos \alpha_1 + y r_2 \cos \alpha_2')/\Omega_1 \sin \alpha_1$, ft^{-1}
B	a parameter, $2\pi r_2^2/60$, sq ft
b	blade height, in.
c	blade chord, in.
d_h	hydraulic diameter, $2 sb/(s + b)$, in.
f	Fanning friction coefficient (average value of 0.004)
g	acceleration due to gravity (at sea level equal to 32.17), ft/sec^2
g_c	dimensional conversion factor, 32.17 (lb mass)(ft)/(lb force)(sec^2)
HP	horsepower
Δh	change in static head, ft
I	moment of inertia, 0.2164 (ft)(lb)(sec^2) for the Mark IX turbopump rotor assembly
j	a numerical used in summations
k_{BS}	bearing and seal resisting torque coefficient, $\rho Q_B^2 \sum_{j=1}^{n} A_j$ at breakaway point (N = 0), $0.75 \rho Q_B^2 \sum_{j=1}^{n} A_j$ at any other point, ft-lb
$k_{f,r}$	rotor frictional loss coefficient, $4f(c_r/d_{h,r})$
$k_{f,s}$	stator frictional loss coefficient, $4f(c_s/d_{h,s})$
k_{PL}	pressure loss resisting torque coefficient, $g_c M_{PL}/g\rho^2 Q^2$, $(ft)(sec^2)/lb$
k_r	rotor inlet loss coefficient, $\sin(\alpha_{1,d}' + \alpha_1)/\sin \alpha_{1,d}'$
k_s	stator inlet loss coefficient, $\sin(\alpha_2' + \alpha_{2,d})/\sin \alpha_{2,d}$

[redacted]

k_W windage resisting torque coefficient, $\left\{\frac{1}{g_c}\sum_{j=1}^{n}\left[B\frac{N}{Q}-A\right]_j-\frac{k_{BS}}{\rho Q^2}\right\}\frac{\rho Q^2}{N^2}$ at steady windmilling, (ft)(lb)(sec^2)

M torque, ft-lb

N rotational speed, rpm

$\dot{N}$ rate of change of rotational speed, rpm/sec

n number of stages

P total pressure, psi

p static pressure, psi

Δp change in static pressure, psi

Q volume flow rate, cu ft/sec

Q_B volume flow rate at breakaway, cu ft/sec

R universal gas constant, ft-lb/(lb)(^oR)

r mean blade radius from axis of rotation, ft

s blade spacing, in.

T absolute temperature, ^oR

u rotor speed at mean blade diameter, ft/sec

V fluid velocity, ft/sec

W work, ft-lb/lb

$\dot{w}$ flow rate, lb/sec

y proportionality constant, V_2'/V_1

α fluid angle, angle between flow direction and tangential direction, deg

λ a polynomial relating tank pressure to pressure drop

ρ fluid density, lb/cu ft

Φ viscous loss term, ft-lb/lb

φ a function

Ω flow area, equal to (1 - blockage) times annulus, sq ft

Subscripts:

ACC	acceleration
a	axial component
BS	bearing and seal
d	design
F	fluid
i	turbine inlet
n	number of stages
o	turbine outlet
PL	pressure loss
r	rotor
s	stator
T	tank
t	turbine
u	tangential component
W	windage
1,2	stage rotor inlet and outlet (see fig. 10(a) for stations)

Superscript:

'	relative to rotor

[redacted]

APPENDIX B

ANALYTICAL EVALUATION OF STARTUP HEAD, FLUID TORQUE, AND ACCELERATING TORQUE CHARACTERISTICS OF A PUMP

The following analysis describes the startup characteristics of an axial pump in terms of head (pressure) and torque parameters. A discussion concerning the degree of accuracy of this analysis is also presented.

Head Characteristic

The energy equation for an incompressible and nonconducting fluid, and for a steady, adiabatic turbulent flow, where the change in potential energy due to change in height is neglected, is (ref. 5)

$$\Delta h = + \frac{\Delta V^2}{2g} + \frac{g_c}{g} W + \frac{g_c}{g} \Phi \qquad (B1)$$

which states that the change of head equals the change of the kinetic energy (based on the average conduit velocity), the work done on the rotor W and the viscous losses Φ (the energy that is dissipated due to viscous effects per pound of fluid). The low-velocity hydraulic turbine flow criteria and a one-dimensional analysis, similar to the approach used in reference 6, are used to describe the flow dynamics of the system under consideration.

Work done by the fluid on the rotor and fluid torque acting on the rotor are considered negative. To expand the right hand side terms of equation (B1), use will be made of the fluid velocity components over blades as shown on figure 9. For simplicity, in the subsequent equations, the parameter g_c will be replaced by g.

Change in kinetic energy. - The change in kinetic energy is completely described by the pump-inlet and the pump-outlet velocity head difference $-\left[(V_2^2)_n - (V_1^2)_{n=1}\right]/2g$ where $(V_2)_n$ is the exit velocity from the last stage rotor of the pump and $(V_1)_{n=1}$ is the inlet velocity to the first-stage rotor.

Work. - The work done by the fluid on the rotor must be described by the individual stage characteristics. If stages are not identical, each stage characteristic must be calculated. A summation of particular stage contributions will yield the overall effect. It will be assumed that each stage fully contributes to the work done to accelerate or keep the pump rotor rotating. This assumption is based on the observation that there is a very low level of energy transfer during windmilling and that every single stage is changing the fluid flow condition and the pressure by a small increment only. The work done on the blades, by Euler's equation, equals $-(u_1 V_{u,1} - u_2 V_{u,2})/g$.

Frictional losses. - The losses resulting from flow through stages are of

[redacted]

two types: losses due to friction and losses due to turbulence induced by the mismatch of blade and flow angles caused by the off-design operation. The frictional losses in variable area conduits are usually based on average fluid velocities. The resulting error will be small because the exit and the average velocities differ very little and, the frictional losses during startup are small compared to all other losses. The stator frictional loss equation will contain the rotor inlet velocity V_1, which is equal in both magnitude and direction to the stator exit velocity. The frictional loss for each stator and rotor is respectively:

$$-\left(4f\,\frac{c_s}{d_{h,s}}\,\frac{V_1^2}{2g}\right) = -\left(k_{f,s}\,\frac{V_1^2}{2g}\right)$$

$$-\left(4f\,\frac{c_r}{d_{h,r}}\,\frac{V_2'^2}{2g}\right) = -\left(k_{f,r}\,\frac{V_2'^2}{2g}\right)$$

where c is the mean-diameter blade length (chord) and d_h is the hydraulic diameter of a rectangular fluid passage formed by the blade spacing s and the blade height b. For converging passages (mixed flow stages) average values for s and b may be used. The friction coefficient f is taken to be 0.004, an average value over a wide range of Reynolds numbers (ref. 5), because as noted, the frictional losses are small.

Turbulence losses. - The turbulence losses which occur at the blade inlet of both rotor and stator rows may be derived by analyzing the rotor inlet and outlet velocity triangles. These triangles also define stator flow diagrams.

An efficient stage operation implies a smooth fluid entrance into the rotor, that is, the fluid angle α_1' will equal the design angle $\alpha_{1,d}'$. At off-design conditions, $\alpha_1' \neq \alpha_{1,d}'$. Consider an arbitrary impeller inlet velocity triangle XYZ as shown in figure 23. The fluid approaches the blades with a relative velocity V_1' at an angle α_1'. Because $\alpha_1' < \alpha_{1,d}'$ a tangential velocity component of adjustment ZZ' will be required to force the fluid to follow the blades. The energy loss resulting from this change of direction equals $-(ZZ')^2/2g$. From the geometry of the trapezoid XYZ'Z above

$$ZZ' = u_1 - \frac{\sin(\alpha_{1,d}' + \alpha_1)}{\sin \alpha_{1,d}'} V_1 = u_1 - k_r V_1$$

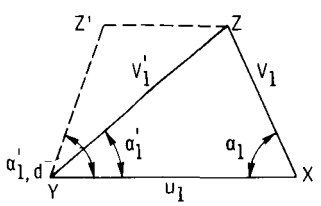

Figure 23. - Impeller inlet velocity triangle at off-design operation.

and the loss is

$$-\frac{(u_1 - k_r V_1)^2}{2g}$$

Similarly the stator entrance loss, which may be evaluated in terms of the rotor outlet relative velocity V_2' and of the mean blade speed u_2 is equal to

[redacted]

$$- \frac{(u_2 - k_s V_2')^2}{2g}$$

where

$$k_s = \frac{\sin(\alpha_2' + \alpha_{2,d})}{\sin \alpha_{2,d}}$$

Generalized head characteristic. - By use of the relations obtained for the work done and for the various losses, equation (B1) becomes

$$2g\,\Delta h = (V_1^2)_{n=1} - (V_2^2)_n - \sum_{j=1}^{n} \left[(k_{f,s} V_1^2 + k_{f,r} V_2'^2)j + 2(u_1 V_{u,1} - u_2 V_{u,2})j \right.$$

$$\left. + (u_1 - k_r V_1)^2 j + (u_2 - k_s V_2')^2 j\right] \qquad (B2)$$

where n is the number of stages.

To express the head loss in terms of V_1 and u_1 only, the following relations, derived from the velocity triangles on figure 9(b) p. 16, will be used:

$$V_{u,1} = V_1 \cos \alpha_1$$

$$V_{u,2} = u_2 - V_2' \cos \alpha_2'$$

$$V_2^2 = u_2^2 + V_2'^2 - 2u_2 V_2' \cos \alpha_2'$$

In addition, it will be convenient to eliminate V_2' by writing $V_2' = yV_1$ where y is a proportionality constant. The two velocities V_2' and V_1 are always proportional to each other because their orientation is fixed, for any given deviation, by the rotor and stator blade angles. Now since $N = 60/(2\pi r)u$ and since the continuity equation states that $Q = \Omega_1 V_1 \sin \alpha_1$, the head equation may be written in measurable quantities such as revolutions per minute N and rate of flow Q instead of the corresponding velocities u_1 and V_1.

After substituting and rearranging, the pump head parameter $\Delta h/Q^2$ of the pump is expressed as a function of the speed parameter N/Q, a number of design parameters, the flow angles α_1 and α_2' and the rotor inlet flow area Ω_1 as

[redacted]

$$\frac{\Delta h}{Q^2} = \left(\frac{1}{2g\Omega_1^2 \sin^2\alpha_1}\right)_{n=1} - \left[\frac{y^2}{2g\Omega_1^2 \sin^2\alpha_1} - \frac{\pi y r_2 \cos\alpha_2'}{30g\Omega_1 \sin\alpha_1}\left(\frac{N}{Q}\right)\right.$$

$$\left. + \frac{\pi^2 r_2^2}{1800g}\left(\frac{N}{Q}\right)^2\right]_n - \sum_{j=1}^{n}\left\{\frac{k_{f,s} + y^2 k_{f,r} + k_r^2 + y^2 k_s^2}{2g\Omega_1^2 \sin^2\alpha_1}\right.$$

$$+ \frac{\pi r_1\left(\cos\alpha_1 + y\frac{r_2}{r_1}\cos\alpha_2' - k_r - y\frac{r_2}{r_1}k_s\right)}{30g\Omega_1 \sin\alpha_1}\left(\frac{N}{Q}\right)$$

$$\left. + \left[1 - \left(\frac{r_2}{r_1}\right)^2\right]\frac{\pi^2 r_1^2}{1800g}\left(\frac{N}{Q}\right)^2\right\}_j \qquad \text{(B3)}$$

This is the final, general expression for the windmilling head characteristic. It is applicable to any type of centrifugal, mixed flow or axial pump, or to a hydraulic turbine. This equation could be solved directly for $\Delta h/Q^2 = \varphi(N/Q)$ if the variations of the two angles α_1 and α_2' and of the area Ω_1 with N/Q are known. The two angles depend on the amount of deviation (see fig. 9(a), p. 16), which is a function of the flow rate Q. The flow area Ω_1 also varies with N/Q because the blockage, due to the boundary layer, varies with Q. There is, generally, a lack of information on the nature of the variation of the deviation and of the blockage with flow in pumps. The difficulty may be bypassed by observing that the deviation may be considered to vary between the design point deviation and zero deviation, although actually it is known from compressor data that at very low flows the deviation may exceed the design point deviation. It will be convenient not to consider those unusual deviations about which there is little or no information and which are limited exclusively to gas flow experiments. Assuming that the blade angles (zero deviation) determine the upper limit for α_1 and α_2' and that the lower limit on those angles will be fixed by design flow angles shown on figure 9(b), it is possible to calculate the limiting head characteristics between which the experimental data are expected to fall.

Because of the lack of data on the variation of blockage with the rate of flow, a constant flow area (the design-point value) will be assumed. In any future analysis, Ω_1 may be made a function of Q if sufficient empirical evidence will quantitatively link the blockage with the flow rate.

Point of zero work done on rotor. - By equating to zero the work term of the head characteristic (eq. (B2)) and after proper substitutions and rearrangement, the value of the speed parameter N/Q for the zero-work point may be calculated from

$$\sum_{j=1}^{n} (u_1 V_{u,1} - u_2 V_{u,2})j = \sum_{j=1}^{n} \left[\frac{Q}{\Omega_1 \sin \alpha_1} (r_1 \cos \alpha_1 + r_2 y \cos \alpha_2') - \frac{\pi r_2^2}{30} N \right] j = 0 \qquad (B4)$$

The point of zero work done on rotor is also a point of zero torque. It is a point of equilibrium beyond which the pump cannot accelerate and where the ratio N/Q has a fixed theoretical value.

Fluid Torque Characteristic

By definition, the available torque in a stage equals the product of the radius, the change of tangential velocity and the mass rate of flow; the total available fluid torque will result from the summation of individual stage torques

$$M_F = \frac{\dot{w}}{g} \sum_{j=1}^{n} (r_2 V_{u,2} - r_1 V_{u,1})j \qquad (B5)$$

Using the same type of transformation as applied to the head characteristic and observing that $\dot{w} = Q\rho$, equation (B5) becomes

$$\frac{M_F}{\rho Q^2} = \frac{1}{g} \sum_{j=1}^{n} \left(\frac{\pi r_2^2}{30} \frac{N}{Q} - \frac{r_1 \cos \alpha_1}{\Omega_1 \sin \alpha_1} - \frac{y r_2 \cos \alpha_2'}{\Omega_1 \sin \alpha_1} \right) j \qquad (B6)$$

which can be also written, in a simplified form as

$$M_F = \frac{\rho}{g} \sum_{j=1}^{n} (BQN - AQ^2)j \qquad (B7)$$

where A and B are composite coefficients. The fluid torque parameter $M_F/\rho Q^2$ is a linear function of the speed parameter N/Q. It also depends on the degree of deviation (by angles α_1 and α_2') and on the amount of blockage in the flow (by area Ω_1). Because the changes in the deviation and in the blockage with the flow rate Q are not determinable at the present time, equation (B6) will be solved by assuming two boundary conditions between which experimental data should fall. The approach presented in the Head Characteristic section is applicable to the solution of the available torque equation (B6).

The theoretical point of zero torque of a startup may be obtained by equating equation (B6) to zero.

Accelerating Torque Characteristic

A useful expression is obtained by a torque balance for windmilling turbopump operation:

$$M_F = M_{ACC} + M_W + M_{PL} + M_{BS} \tag{B8}$$

where M_F is the fluid available torque, given by equation (B7).

The terms M_{BS}, M_{PL}, M_W, and M_{ACC} are the bearing and seal friction torques, the pressure loss torque, the windage loss torque, and the accelerating torque, respectively.

The evaluation of these torques is basically empirical and only qualitative assumptions are possible. The bearing and seal resisting torque may be considered independent of the rotational speed, that is, $M_{BS} = -k_{BS}$. The fluid-friction pressure loss produces a tangential component which in turn results in a resisting torque $M_{PL} = -k_{PL}Q^2\rho^2$. The turbine windage loss is proportional to the square of rotation speed $M_W = k_W N^2$. Collecting the various torques and solving for the accelerating torque parameter:

$$\frac{M_{ACC}}{\rho Q^2} = \frac{1}{g}\sum_{j=1}^{n} B\left(\frac{N}{Q} - A\right)j + \frac{k_{BS}}{\rho Q^2} + k_{PL}\rho + \frac{k_W}{\rho}\left(\frac{N}{Q}\right)^2 \tag{B9}$$

Equation (B9) indicates that the accelerating torque parameter does not generalize. It depends on the absolute value of flow and on the fluid density. Furthermore, the coefficient k_{BS} may assume one value for a rotating system (kinetic friction) and a different value, higher, for a stationary system, that is, when the pump rotor is held and static friction is helping to keep it from rotation. Finally, the seal and bearing friction term loses its meaning when flow is zero. For $Q = 0$ it is necessary to put $k_{BS} = 0$. An examination of the magnitude of terms of equation (B8) indicates that $k_{PL}\rho$ is very small compared with other terms and hence that it may be disregarded.

The final equation for the accelerating torque during windmilling reduces to:

$$\frac{M_{ACC}}{\rho Q^2} = \frac{1}{g_c}\sum_{j=1}^{n}\left[B\left(\frac{N}{Q}\right) - A\right]j + \frac{k_{BS}}{\rho Q^2} + \frac{k_W}{\rho}\left(\frac{N}{Q}\right)^2 \tag{B10}$$

with A and B as defined in the available torque equation (B7) and k_{BS} and k_W are empirical constants combining the effects of both bearings and seal friction, and the windage loss.

[redacted]

REFERENCES

1. Connelly, R. E.: Design Study of the Mark IX Pump. Rept. No. R-6254, Rocketdyne, North Am. Aviation, Inc., Mar. 1959.

2. Emmert, H. D.: Thermodynamic Design of the Mark IX Turbine. Rocketdyne, North Am. Aviation, Inc., Mar. 23, 1960.

3. Yee, Theodore: The Torque Transducer, A Device for the Dynamic Measurement of Torque. Rept. No. R-196P, Rocketdyne, North Am. Aviation, Inc., May 1956.

4. Swanson, W. M.: Complete Characteristic Circle Diagrams for Turbomachinery. Trans. ASME, vol. 75, July 1953, pp. 819-826.

5. Knudsen, J. G.; and Katz, D. L.: Fluid Dynamics and Heat Transfer. McGraw-Hill Book Co., Inc., 1958.

6. Daugherty, R. L.: Hydraulic Turbines. Third ed., McGraw-Hill Book Co., 1920.

[redacted]

"The aeronautical and space activities of the United States shall be conducted so as to contribute . . . to the expansion of human knowledge of phenomena in the atmosphere and space. The Administration shall provide for the widest practicable and appropriate dissemination of information concerning its activities and the results thereof."

—NATIONAL AERONAUTICS AND SPACE ACT OF 1958

NASA SCIENTIFIC AND TECHNICAL PUBLICATIONS

TECHNICAL REPORTS: Scientific and technical information considered important, complete, and a lasting contribution to existing knowledge.

TECHNICAL NOTES: Information less broad in scope but nevertheless of importance as a contribution to existing knowledge.

TECHNICAL MEMORANDUMS: Information receiving limited distribution because of preliminary data, security classification, or other reasons.

CONTRACTOR REPORTS: Technical information generated in connection with a NASA contract or grant and released under NASA auspices.

TECHNICAL TRANSLATIONS: Information published in a foreign language considered to merit NASA distribution in English.

TECHNICAL REPRINTS: Information derived from NASA activities and initially published in the form of journal articles.

SPECIAL PUBLICATIONS: Information derived from or of value to NASA activities but not necessarily reporting the results of individual NASA-programmed scientific efforts. Publications include conference proceedings, monographs, data compilations, handbooks, sourcebooks, and special bibliographies.

Details on the availability of these publications may be obtained from:

SCIENTIFIC AND TECHNICAL INFORMATION DIVISION

NATIONAL AERONAUTICS AND SPACE ADMINISTRATION

Washington, D.C. 20546

[redacted]